

Uncovering and Understanding FPR Manipulation Attack in Industrial IoT Networks

Mohammad Shamim Ahsan and Peng Liu *Member, IEEE*

Abstract—In the network security domain, due to practical issues – including imbalanced data and heterogeneous legitimate network traffic – adversarial attacks in machine learning-based NIDSs have been viewed as *attack* packets misclassified as *benign*. Due to this prevailing belief, the possibility of (maliciously) perturbed *benign* packets being misclassified as *attack* has been largely ignored. In this paper, we demonstrate that this is not only theoretically possible, but also a particular threat to NIDS. In particular, we uncover a practical cyberattack, *FPR manipulation attack* (FPA), especially targeting industrial IoT networks, where domain-specific knowledge of the widely used MQTT protocol is exploited and a systematic simple *packet-level* perturbation is performed to alter the labels of benign traffic samples *without* employing traditional gradient-based or non-gradient-based methods. The experimental evaluations demonstrate that this novel attack results in a success rate of 80.19% to 100%. In addition, while estimating impacts in the Security Operations Center, we observe that even a small fraction of false positive alerts, irrespective of different budget constraints and alert traffic intensities, can increase the delay of genuine alerts investigations up to 2 hr in a single day under normal operating conditions. Furthermore, a series of relevant statistical and XAI analyses is conducted to understand the key factors behind this remarkable success. Finally, we explore the effectiveness of the FPA packets to enhance models’ robustness through *adversarial training* and investigate the changes in *decision boundaries* accordingly.

I. INTRODUCTION

In the critical field of network security, the expected performance of a network intrusion detection system (NIDS) is determined through the *operation point*, i.e., the selected FNR-FPR (False Negative Rate-False Positive Rate) tradeoff point on the ROC (Receiver Operating Characteristic) curve, chosen by the Security Operations Center (SOC) during deployment. However, **operation point drift**, induced by adversarial attacks, could result in a significant deviation from expected performance. Therefore, investigating operation point drift is paramount to gain awareness of the real NIDS performance.

When successful adversarial evasion attacks [1], [2], [3], [4], [5], [6], [7], [8], [9] are in presence, the previously-chosen operation point would drift to a new position in the ROC space where the x-axis represents the FPR, while the y-axis represents the TPR (True Positive Rate). Because the evasion attacks result in false negatives, the drifting direction would be up-and-down, that is, the new position has a smaller y-coordinate, but the x-coordinate remains unchanged. Although drifting along the side-to-side direction is theoretically possible, only up-and-down drifting has been reported in the literature.

Mohammad Shamim Ahsan and Peng Liu are with the College of Information Sciences and Technology, Pennsylvania State University, University Park, PA 16801 USA. (email: msa6152@psu.edu, pxi20@psu.edu)

In this paper, we demonstrate that *side-to-side operation point drifting is not only theoretically possible, but also a practical threat to NIDS effectiveness*. The demonstration is achieved through a newly uncovered **FPR manipulation attack** (FPA, in short) against machine learning-based NIDSs defending industrial internet of things (IIoT) networks. Regarding whether this is a profound research finding, our main observations are associated with not only signature-based NIDS but also ML-based NIDS.

First of all, we found that FPR manipulation attack can indeed result in very serious real-world consequences, particularly the investigations of genuine threats can drastically be hampered, making the network more vulnerable to actual attacks. Our experiments, conducted in §V-C, show that a relatively small number of false alarms caused by FPA can lead to **several hours of delay** in investigating genuine alerts, even under normal cyber operation conditions.

Second, from the point of view of signature-based NIDS (e.g., Snort [10], Bro [11]), although benign traffic could be theoretically perturbed while remaining benign and cause NIDS to raise false alarms, a signature-based NIDS usually does not provide realistic opportunities for such perturbations to succeed. In particular, signature-based NIDSs have one property: there is a notable distance between the clean, precise signatures and slightly perturbed benign traffic. Consequently, slight perturbations without violating any network protocol constraints are *unlikely* to result in a considerable deviation.

Third, from an ML-NIDS perspective, researchers tend to treat “adversarial examples” and “attack packets” equivalently, though this belief does have a **logic gap**, since *benign packets could also serve as adversarial examples* in the ML context. Many researchers are probably aware of this logic gap, but it is clear that the logic gap has not been taken seriously. Reflecting on why it has not been received sufficient attention, we found two possible reasons: (Reason 1) ML-based NIDS is often developed to address the limitations of signature-based NIDS, but as mentioned above, slightly perturbed benign traffic is unlikely to trigger a signature-based NIDS to raise alarms. (Reason 2) Due to several real-world considerations, researchers tend to assume that evasion attacks are more realistic than FPR manipulation attacks. Here, we illustrate two such real-world considerations. (a) *Imbalanced data* is a widely existing issue for ML-based NIDS [12], [13], [14]. Since the amount of benign packets is usually much greater than that of attack packets in the training dataset, researchers are of the view that the trained model has more vulnerabilities (e.g., overfitting) associated with attack packets. (b) Due to heterogeneous protocols and applications, benign packets in

IoT networks exhibit *diversity*, which enables a detection model to learn more generalized underlying structures of these packets and makes adversarial perturbations less likely to succeed. For example, Edge-IIoTset [15], the most widely-adopted benchmark IIoT network dataset in the research community, has one interesting characteristic: although about 20% of the benign packets are MQTT packets, none of the (fourteen) attack classes involve MQTT packets. As a result, the trained model pushes the *decision boundary* far away from the cluster of MQTT samples. In fact, we checked the margins computed from the logits (pre-softmax) of the final dense layer, following the standard approach [16], and found that all (correctly) classified MQTT packets have very large positive margins (roughly 120~124), eventually predicted with near-perfect confidence scores. This indicates that they lie far from the decision boundary; hence, highly robust to *minimal* perturbations [17], [18], [19].

Finally, the importance of this research finding is also due to the **practicality** of the newly uncovered FPR manipulation attack. Based on the surprising finding that *a systematic simple perturbation of real MQTT packets is sufficient to flip the label of the unperturbed versions*, our FPR manipulation attack does not require one to apply any sophisticated attack techniques, such as gradient-based [4], [5], [20], [21], [22], score-based [6], [23], decision boundary-based [6], [24], or GAN-based approaches [1], [2], [3], [25]. In addition, since FPR manipulation attacks only utilize benign and legitimate MQTT messages, the new attack, in principle, is hard to detect. Moreover, the adversary often employs multiple IoT devices to attack the network and can tactically avoid letting the same device launch both evasion attacks and FPR manipulation attacks. This makes the new attack even harder to detect.

Overview of the new attack. The FPR manipulation attack (FPA, in short) leverages an adversary's domain knowledge of the MQTT (Message Queuing Telemetry Transport) protocol, widely used in real-world IIoT environments due to its fast, lightweight, and reliable data transfer facility [26]. In MQTT communication, a set of *control* packets, such as CONNECT, CONNACK, SUBSCRIBE, PUBLISH, etc., is used to ensure secure and flexible integration. An IIoT device - for example, a temperature and humidity sensor - can connect as an MQTT client and publish its sensor readings to the server, which then forwards them to subscribed clients. In this paper, the FPA attack is launched from the IIoT device in a similar setting, assuming the device (i.e., publisher) is already compromised. In particular, the attacker systematically designs MQTT PUBLISH packets, keeping the network and protocol requirements intact, and sends them to the MQTT server. Upon receiving, the server responds as specified by the protocol. However, ML-based NIDS, which continuously monitors the network, becomes confused and confidently misclassifies MQTT traffic sent from the device and triggers a false threat alarm. From a security analyst's point of view, the crafted MQTT packets are *benign*, since they neither provoke any malicious behavior nor carry any harmful information; rather, they contain relevant sensor readings. However, FPA is

an attack in the sense that it misleads the neural network and induces false alarms in the system, **intentionally** disrupting the normal workflow of the SOC.

Contributions. In summary, this paper has made the following contributions.

- We propose a novel cyberattack, called *FPR manipulation attack* (FPA, in short), especially targeting Industrial Internet of Things (IIoT) networks. In particular, the attacker exploits domain-specific knowledge of the predominant MQTT protocol and systematically designs harmless and valid network packets that are misclassified by top-notch machine learning-based network intrusion detection systems (ML-NIDSs). To the best of our knowledge, no prior work has investigated such an attack in this setting.
- We conduct thorough experiments on several public ML-NIDSs. The experimental results demonstrate that FPA achieves **80.19% – 100%** attack success rate across these models. Notably, in a significant number of cases, the models show **overconfidence** during incorrect predictions. In addition, a minimal proportion of FPA attack significantly delays the investigation of genuine alerts in the Security Operations Center - roughly from **56.37 sec** to **154.32 sec** in one hour, and from **9.49 hr** to **11.41 hr** in a single day - regardless of standard budgets and alert traffic intensities.
- We explore popular statistical metrics and explainability (XAI) methods and find a **distributional shift** in the FPA attack samples away from the benign ones. Additionally, an **overlap** is observed between the FPA cluster and the true attack class in the internal representation of the models.
- Finally, we adopt *adversarial training* as a defense against the attack, and observe that although it can correctly classify FPA packets, the per-class performances of several true attack classes are drastically decreased. This observation corroborates the findings from our *decision boundary analysis*.

II. BACKGROUND

A. MQTT Protocol

MQTT (Message Queuing Telemetry Transport) is a client-server publish/subscribe protocol efficient for fast and reliable data transfer in constrained environments such as the Industrial Internet of Things (IIoT), where devices have limited processing power and network bandwidth [26]. This lightweight protocol typically runs over TCP/IP, and both clients and server (a.k.a. broker) need to have a TCP/IP stack. During data transfer, MQTT clients cannot directly communicate with each other; the server always serves as a mediator. Each application message contains a label, known as *topic*). Whenever a client publishes a message on a specific topic, the server sends copies of the message to the clients who have already subscribed to that topic.

B. MQTT Control Packet Format

The MQTT protocol provides 14 different types of control packets, among which CONNECT, PUBLISH, SUBSCRIBE, and DISCONNECT are frequently used. An MQTT control packet consists of three main parts: fixed header, variable header, and payload. The fixed header is available in each type of control packet, whereas the existence of a variable header and payload varies across different packets. A fixed header can be 2~5 bytes long, depending on the message. The first byte comprises a set of control bits. The next 1~4 bytes of the fixed header, starting from byte two, contain the length of the variable header and payload, known as the *Remaining length*. This flexible formatting allows applications to send control packets of size up to 256 MB ($2^{28} - 1$). Typically, each subscription- or publish-related message contains a packet identifier in the variable header. However, payload is present only in CONNECT, PUBLISH (optional), SUBSCRIBE, SUB-ACK, and UNSUBSCRIBE messages.

III. THREAT MODEL

Attack scenario. Figure 1 illustrates the threat model of the proposed FPR manipulation attack. The model consists of an MQTT client, an MQTT broker/server, a router, a deep packet inspection (DPI) tool, and a security operations center (SOC). In the SOC, an ML-based NIDS is deployed to extract features from raw network traffic and perform a classification task. The client is an IIoT device compromised prior to launching the attack. The server (a.k.a., broker¹) can be an edge server, cloud broker, or embedded component within a gateway device. Since an edge server is ideal for industrial IoT settings, it is assumed that the server resides within the internal industrial network. To offer efficient and secure communication between publishers and subscribers, this server maintains a set of access control policies to grant clients read, write, or both operations to messages referring to defined topics [27]. A read access corresponds to the right to receive messages on subscribed topic(s); whereas a write authorization indicates permission to publish messages to the allowed topic(s). To facilitate hierarchical access, avoid redundancy, and smooth policy management, an industrial MQTT server commonly uses *single-level* or *multi-level wildcards*, especially single-level [28], [29], [30]. Example usage of wildcards in ACL is provided in the Appendix (§A).

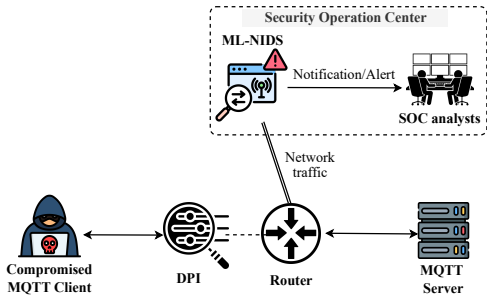


Fig. 1. Threat model of FPR manipulation attack

¹In this work, we prefer to use the term “Server”, instead of “Broker”

A router acts as the gateway to forward each client’s MQTT network packets to the MQTT server and forward the response packets back to the client. From the perspective of network firewalls and DPI, this traffic is generally first inspected by a packet filtering device or tool before being handled by the router. Regarding firewalls, traditional ones filter based on protocol header fields, specifically IP addresses, ports, network interface, and specific transport layer and IP header fields [31], [32]. In contrast, DPI is an additional capability, often integrated with stateful firewalls to inspect both communication headers and actual data or code payloads [33], [34]. After inspecting both the headers and content of the MQTT packet, if the packet is not blocked, the packet will arrive at the router, where the router’s hardware will capture each packet in a pcap file. Then, the pcap file will be transferred to the SOC. A machine learning-based NIDS, located in the SOC, extracts features from traffic and detects both benign activities and potential threats of attacks. In case of an attack, ML-NIDS sends alerts to security analysts, who then manually investigate whether the alerted packets/sessions are indeed a malicious act.

Assumptions. First, we assume that *at least* one IIoT device within the targeted network has already been compromised, which serves as the MQTT client during the FPA attack. Since this device is authorized on the network, the DPI does not block any legitimate packets originating from the device (see Figure 1). Second, to regulate topics on the access control list, the MQTT server uses single-level wildcard (+), a common industry practice to ensure flexibility and security [28], [29], [30]. Notably, we avoid the assumption of using the multi-level wildcard (#), as it can provoke illegal manipulations throughout MQTT networks [35]. The final assumption is that the machine learning-based NIDS is trained offline prior to deployment. However, it can perform near-real-time detection during the attack.

Attacker’s capability. We consider a *black-box* setting, i.e., the attacker does not have access to the architecture and parameters of the target model. In addition, the training data and the features extracted from raw network traffic during training are also unknown to the attacker. However, he knows that pcap files are used as input to the ML-NIDS. This characteristic allows our attack to be *generic*: the attack can be launched to confuse a variety of detection models developed to protect industrial IoT networks.

To successfully execute the attack, the attacker must satisfy the IID (independent and identically distributed) assumption underpinning the ML model [36]. In particular, this principle states that the data samples used during the development of ML-NIDS must be similar to those that the model analyzes after deployment. In short, the feature set, its distribution, and domain must be identical before and after deployment. Since the proposed FPR manipulation attack relies on specially crafted MQTT packets in an IIoT environment, the attack is *valid* as long as it maintains the network and protocol constraints and does not introduce anything harmful to the system.

IV. PROPOSED FPR MANIPULATION ATTACK

A. Attack Overview

Figure 2 illustrates an overview of the proposed FPR manipulation attack (FPA). Specifically, an attacker needs to perform the following two steps to carry out this attack.

- 1) Use a compromised IIoT device to establish an MQTT connection handshake by carefully sending a CONNECT packet. Before that, creating a TCP connection is required as MQTT operates over the TCP/IP stack.
- 2) Strategically craft the *payload* and *topic* of the MQTT PUBLISH packets and send them to the server.

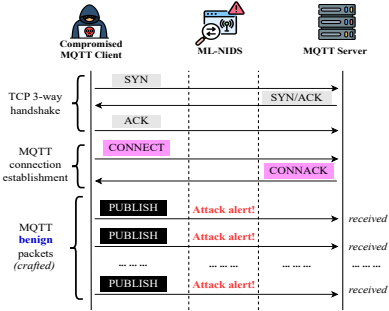


Fig. 2. Overview of FPR manipulation attack

B. Pre-condition: Initiate MQTT Connection

As MQTT operates over TCP/IP, the attacker first sends a SYN packet from a compromised IIoT device to initiate a TCP connection and then completes the standard three-way handshake to establish a session.

According to Section 3.1 of the MQTT-v3.1.1 spec [26], the first MQTT packet must be a CONNECT message, and a client is restricted to sending only one such packet. Subsequently, the attacker sends one CONNECT request to the MQTT server immediately after establishing the TCP connection. It is important to note that, while the CONNECT control packet is *not* considered as a central part of the FPR manipulation attack, it must be carefully formatted to successfully create an MQTT session. The fixed header of the CONNECT message specifies the control type, so it cannot be customized. The first seven bytes of the variable header are also protocol-related (see Figure 3), specifically: protocol name (MQTT), protocol length (size of the protocol name string), and protocol level (0x04, fixed for MQTT-v3.1.1). Any discrepancy in these fields certainly results in the rejection of connection establishment. However, the next byte, *Connect flags*, is modifiable. In particular, this byte consists of the User Name Flag, Password Flag, Will Retain, Will QoS, Will Flag, Clean Session, and a Reserved bit, arranged from bit 7 to bit 0, respectively. Since the MQTT client is already compromised, the attacker can set the username and password flags to one and seamlessly authenticate to the server. Will-specific flags are used to configure whether the client wants the server to notify other clients if the client disconnects or dies unexpectedly without a DISCONNECT request. Because these bits are irrelevant to the attack, they are set to zero. The Clean Session provides

Fixed Header								
Bit	7	6	5	4	3	2	1	0
byte 1	Control Packet type (1) Reserved (0)							
byte 2-5	Remaining Length							
Variable Header								
byte 1-2	Protocol Length (4)							
byte 3-6	Protocol Name (MQTT)							
byte 7	Protocol Level (0x04)							
byte 8	Connect Flags							
byte 9-10	1	1	0	0	0	X	0	
Keep Alive (XX)								
Payload								
Client Identifier								
Username								
Password								
varied								

Fig. 3. Format of an MQTT CONNECT packet

a server with the ability to resume the previous session and store the current one based on the client identifier. However, the proposed attack works for either case, as it is independent of sessions (represented as 'X' in Figure 3). According to Section 3.1.2 of the MQTT-v3.1.1 spec [26], the reserved flag of a CONNECT control packet must be zero; otherwise, the server will declare it as an invalid request. The last two bytes of the variable header are called Keep Alive (see Figure 3). It is used to measure the maximum allowed time interval (in seconds) between two consecutive control packets sent by the client (attacker). Whenever this threshold is exceeded without any control message or PINGREQ, the server terminates the session. Although a client can set this up to 65535, MQTT servers often set a limit or override it in the real world [29]. However, to avoid unexpected events, it is better to set this value to zero. Notably, the proposed attack is not constrained by any specific Keep Alive value, as the attacker can consistently send control packets (especially, PUBLISH) or keep the session active using PINGREQ packets. Regarding the payload of the CONNECT control message, its length is varied as the client identifier, username, and password are user-defined. The first two fields contain UTF-8 encoded strings, while the Password field contains binary data ranging from 0 to 65535 bytes. However, the payload would be larger if the Will flags were set to one.

After sending the carefully-structured CONNECT packet, the server responds with a CONNACK message containing a return code "0x00" (rc0), which is an indication of successful connection.

C. Execution: Send Crafted MQTT PUBLISH Packets

This is the core phase of the FPR manipulation attack, where the attacker designs custom PUBLISH messages (or *FPA packets*, in formal). These packets must adhere to domain-specific constraints so that they can pass through deep packet inspection tools and ultimately deceive ML-NIDS. Specifically, three fields - control flags, topic name, and payload - are deliberately crafted. However, designing control flags is not directly related to the attack; instead, it is essential to continue the attack without any unexpected disruption discussed below.

① Control Flags Configuration. The four leftmost bits of the fixed header indicate control packet type, which is fixed to '3' for a PUBLISH packet (see Figure 4). The attacker does not need to ensure redelivery, so the DUP flag is set to zero. For QoS bits, special care is needed, especially while setting

QoS=2 (the highest QoS), as it requires a four-way handshake (i.e., PUBLISH→PUBREC→PUBREL→PUBCOMP) to complete the packet flow. However, our crafted packets do not contain QoS=2, since including it would introduce unnecessary complexity in realistic attack testing. Additionally, QoS=1 inherits the restriction of an additional field (i.e., packet identifier) in the variable header, and generating it is not an arduous task for the attacker. Moreover, for a PUBLISH packet with QoS=1, the server responds with a PUBACK packet, an indicator of successful acceptance of the crafted packet. Furthermore, the attacker must not set both QoS bits to one, as prohibited by the protocol [MQTT-3.3.1-4] [26]. Regarding the RETAIN flag, setting it to one forces the server to store the PUBLISH message and send it to the clients who will subscribe in the future. Notably, the server stores only one retained message per topic. However, this bit can be set to zero as well, since the attacker does not need to think about future clients. Importantly, if this bit is set to zero and no subscribed client exists for the topic, then the PUBLISH messages are still received by the server (but not stored), and the ML-NIDS continues to observe this traffic. In this way, the first byte of the fixed header becomes either “0x30”, “0x31”, “0x33”, or “0x35”. The next bytes of this header, *Remaining Length*, depend on the rest of the contents, and so the attacker does not need to put extra effort to adjust them.

② Topic Generation. Second, the attacker aims to generate topics in an intuitive way. Here, two key aspects must be considered: (i) the protocol constraints, and (ii) the access control policies of the MQTT server. A *topic name* is a UTF-8 encoded string structured as a sequence of alphanumeric characters and must not be encoded to more than $2^{16} - 1$ bytes. It can consist of a hierarchical topic structure with several levels separated by “/” (a.k.a., topic level separator). According to Section 3.3.2.1 of OASIS MQTTv3.1.1 spec [26], a topic name in an MQTT PUBLISH packet cannot contain any wildcard character (e.g., +, #) and cannot start with “\$”. However, the Access Control List (ACL) can contain such wildcards. Although using hierarchical topics is optional, the single-level wildcard (+) is widely used in large-scale industries to ensure adaptive and scalable topic management for both publishing and subscription [28], [29], [30]. For example, an ACL in the server-side containing `topic write Building1/Floor3/+` for a specific user indicates that the authorized client is allowed to publish any topic that matches the pattern `Building1/Floor3/<subtopic>`, where `<subtopic>` can be any single-level wildcard (e.g., `Building1/Floor3/Sensor1`, `Building1/Floor3/Sensor2`, etc.). However, topics with more than one level, such as `Building1/Floor3/<subtopic_1>/<subtopic_2>` or `Building1/Floor3/<subtopic_1>.../<subtopic_n>` will be declined by the server. In this way, PUBLISH messages from a group of IIoT devices operating on a specific floor or building can be seamlessly handled. In addition, it also signifies that clients from other floors or buildings are not permitted to publish to this topic. Consequently, subscribed clients receive appropriate messages from authentic publishers. Observing such effective practical applications, we utilize

the single-level wildcard for the topics. However, the use of multi-level wildcard (#) is not considered, since it is not ideal for secure industrial networks [35].

Bit	7	6	5	4	3	2	1	0
byte 1	Control Packet type (3)		DUP (0)	QoS (XX)	RETAIN (X)			
byte 2-5			Remaining Length					
<i>Variable Header</i>								
byte 1-2			Topic Length					
byte 3-N			Topic Name					
byte N+1-N+2			Packet Identifier (QoS>0)					
<i>Payload</i>								
varied			Application message					

Fig. 4. Structure of a crafted MQTT PUBLISH packet

In particular, a streamlined *whitespace padding* strategy is applied to extend the existing topic names, while preserving the same hierarchical topic structure. To explain this padding and its rationale, we briefly restate the primary objective of the FPR manipulation attack: craft *benign* MQTT packets so that the ML-NIDS located in the security operations center incorrectly classifies them as *malicious*. To accomplish a successful attack, two crucial factors need to be taken into account. First, the topic name is a categorical feature, as it is a UTF-8 encoded string representing a set of discrete categories in the industrial IoT context. Second, machine learning algorithms can only work with numeric values and must follow the IID principle, which enforces that the feature set, their distribution, and domain must be identical in development and inference [36]. Accordingly, categorical features are often transformed to numeric values using different techniques, such as one-hot encoding, label encoding, and ordinal encoding [37]. In order to break the existing categorical encoded patterns from which the machine learning model has learned, intuitively, only a small set of additional topics is required. Therefore, in this paper, existing topics are extended using n number of whitespace characters (we set $n = [0, 3]$). For instance, “`Building1/Floor3/Sensor1`”, “`Building1/Floor3/Sensor1`”, “`Building1/Floor3/Sensor1`”, and “`Building1/Floor3/Sensor1`” are generated for the existing topic “`Building1/Floor3/Sensor1`”. It is worth noting that the corresponding ACL rule was `topic write Building1/Floor3/+`. Although these newly derived spaced-topics can be ignored or dropped by preprocessing components, during inference, to satisfy the IID principle (which may not always be ideal for a real-world environment), the existing learning patterns are still affected to some extent depending on the importance of the *TOPIC* feature. A conceptual explanation of this impact is provided in the Appendix (§C). It should be noted that although the protocol implicitly allows *blindly* random topics maintaining the access control policy (e.g., `Building1/Floor3/abcde`, `Building1/Floor3/nwcrq`), the attacker avoids doing this to make the topics relevant, non-malicious, and realistic to the security analysts.

③ Payload Construction. Finally, the attacker designs the application message, that is, the payload. Since MQTT does not depend on the specific type or format of data, the attacker has the flexibility to inject text in any encoding, data in binary, images, and even encrypted data as well [38]. In this paper, the

payload is constructed using a similar *padding* technique by adding numerous ‘whitespace’ after the original sensor measurements. However, whitespace cannot be added *blindly* since the network and protocol impose some implicit constraints on payload length. The first restriction is the dependency on the *Remaining Length* field. In particular, the remaining length indicates the combined size of the variable header and the payload (*mqtt.msg*), measured in bytes. Since the crafted variable header can contain the topic length (*topic_len*), topic name (*topic*), and packet identifier (*msgid*) fields, the value of the remaining length (*mqtt.len*) becomes:

$$mqtt.len = topic_len + topic + msgid + mqtt.msg \quad (1)$$

Second, the TCP segment size (i.e., the length of the application data) depends on the value of the Remaining Length field since MQTT operates over the TCP/IP stack. Although an MQTT PUBLISH packet can be at most 268,435,455 bytes long (Section 2.2.3 of MQTT-v3.1.1 [26]), the TCP maximum segment size (MSS) is often 1460 bytes in real-world settings [39], [40]. Based on this threshold, the relation between the TCP segment size (*tcp.len*) and the MQTT remaining length (*mqtt.len*) can be made as follows:

$$tcp.len = \begin{cases} mqtt.len + 2 & \text{if } mqtt.len \leq 255 \\ mqtt.len + 3 & \text{otherwise} \end{cases} \quad (2)$$

In Equation 2, the numbers (+2 and +3) refer to the length of the fixed header in the crafted PUBLISH control packet. For the first case, the *Remaining Length* field requires one byte; whereas, in the latter case, it takes two bytes to fit a value of more than 255. As a consequence, the fixed header becomes two or three bytes, respectively. By combining Equations 1 and 2, the payload - and thus the maximum number of whitespaces allowed for padding - can be rigorously calculated. It is worth noting that although the payload is constructed using plain-text data, an attacker can adapt any data format and its contents according to specific applications.

Arguably, the crafted PUBLISH packets are *benign* indeed because the whitespace characters do *not* affect the content of the payload and *no harmful effects* to the industrial network whatsoever. The main purpose of the proposed padding strategy is to make the length of the PUBLISH packets dynamic, not the content itself. Another noticeable thing is that although the attack explicitly designs the topic name (*topic*) and payload (*mqtt.msg*), some other crucial fields are inherently and automatically changed in the packet due to *intra-packet dependencies* (i.e., the value of one field depends on the values of other fields within a single packet). In our case – the MQTT remaining length, TCP payload (the actual application data), TCP segment size (payload length), TCP checksum, and TCP sequence number – exhibit such intra-packet dependencies. The relations of PUBLISH payload with MQTT remaining length and TCP segment size are described earlier (see Equations 1 and 2). The TCP payload is the main content of the network layer, which certainly contains the MQTT message. The TCP checksum ensures the integrity of a TCP packet by detecting errors during transmission. Specifically, at first, the sender (client) calculates the checksum

and includes it in the packet. Upon receipt, the receiver (server) then recalculates it and compares it to the one in the packet. If they match, the packet is accepted as error-free; otherwise, it is rejected. Since the calculation relies on the TCP payload (Section 3.1 of RFC 793 [41]), this field is also influenced by the FPR manipulation attack. However, it is observed that existing ML-NIDSs typically drop raw payload features, such as TCP payloads and MQTT messages, as they contain a variety of data from different protocols that require high computational cost and are often encrypted [42]. Moreover, models tend to overfit to specific contents and formats and suffer from poor generalization. Regarding the TCP sequence number (*tcp.seq*), it is increased based on the number of data (payload) bytes most recently sent by the client. In particular, the update equation is $tcp.seq_i = tcp.seq_{i-1} + tcp.len_{i-1}$, where i and $i - 1$ respectively denote the current and previous packets in the same direction, and *tcp.len* represents the payload size in bytes (TCP segment size). However, the sequence number is reinitialized for every new TCP session.

V. EVALUATION

In this section, we focus on addressing the following research questions:

- **RQ1: Validation Test.** *Is it possible to craft MQTT control packets as proposed for use in real-world environments?*
- **RQ2: Effectiveness and Impact Analysis.** *How effective are the designed packets to confuse ML-based NIDSs? What is the real-world impact of this attack?*
- **RQ3: Attack Analysis and XAI.** *What are the possible reasons behind the misclassification of FPA packets by ML-NIDSs?*
- **RQ4: Adversarial Training.** *Does the utilization of crafted packets in adversarial training improve the robustness of the detection models?*
- **RQ5: Decision Boundary Analysis.** *How does the decision boundary of the models change after defensive retraining?*

A. Selected ML-NIDSs

To test our proposed FPR manipulation attack (FPA), a key requirement must be satisfied: the ML-NIDS needs to perform considerably for the original uncrafted MQTT PUBLISH packets. In this section, we describe the dataset, the reason behind selecting it, and a brief introduction to the selected ML-NIDSs.

Selection: We select detection systems that are trained on the *Edge-IoTset* (2022) [15] dataset, recognized as the most prominent dataset for IIoT in recent years because of its close replication of real-world industrial settings, absent in other available datasets. The dataset contains network traffic for 14 attack classes (27.2%), along with one benign class (72.8%), both in *pcap* and *csv* formats. In addition, two separate *csv* files are available to train and test machine learning-based NIDSs. The benign traffic is generated using 10 different IoT devices. Among these 1698659 packets of benign traffic, 332075 (~ 20%) packets are MQTT control packets. In terms of features, 61 different packet-level attributes are

extracted in this dataset. These features can be categorized into several protocol-related groups, as outlined in Table V with a corresponding ID assigned. Other widely used datasets - such as NSL-KDD (2009) [43], UNSW-NB15 (2015) [44], BoT-IoT (2019) [45], CICIDS-2017 (2017) [46], TON-IoT (2021) [47], and N-BaIoT (2018) [48] - do not contain any feature related to the MQTT protocol. Moreover, most of these datasets are not simulated in a real-world IIoT environment [15]. For these reasons, the ML-NIDS developed using the Edge-IIoTset dataset is an appropriate choice to test our proposed attack.

Description of the ML-NIDSs: We select four representative ML-NIDSs that are publicly available, well-cited in academia, and demonstrate remarkable performance on original MQTT packets. Although there are a few other public ML-NIDSs, they underperformed on the original MQTT samples and, therefore, are excluded from our evaluation. For other existing works, which are not open-sourced, we contacted the authors of 15 papers, but did not receive any response. However, the first selected ML-NIDS is a CNN and BiLSTM-based model, referred to as *DCNNBiLSTM* [49], a recently popular NIDS in literature. The second ML-NIDS is *CNN-LSTM-GRU* [50], an ensemble classifier that consists of three advanced neural networks. Following that, the third ML-NIDS is a CNN and LSTM-based model (*SF-CNN-LSTM* [51]), enhanced by statistical filtering techniques. Although the last system also integrates CNN and LSTM [52], we choose this one because it is trained solely on transport and network layer features, which helps us better evaluate the effect of FPA. Table VI shows the features used by these ML-NIDSs. Notably, three of these ML-NIDSs use one-hot encoding, while the remaining one adopts label encoding for processing categorical features. The effectiveness of these systems is verified through testing of overall performance, performance on benign samples, and performance on MQTT PUBLISH packets. According to Table I, the overall accuracy, precision, recall, and F1-score are decent ($\sim 95\% - 100\%$), and the metrics for benign cases are remarkable ($\sim 100\%$).

TABLE I
VERIFICATION EXPERIMENTS OF THE SELECTED ML-NIDSs

ML-NIDS	Overall (%)				Benign Packets (%)				MQTT PUBLISH (%)			
	acc	prec.	rec.	F1	acc	prec.	rec.	F1	acc	prec.	rec.	F1
DCNNBiLSTM [49]	99.64	99.66	99.64	99.13	100	100	100	100	100	100	100	100
CNN-LSTM-GRU [50]	97	97	97	97	100	100	100	100	100	100	100	100
SF-CNN-LSTM [51]	94.99	96.21	94.95	94.5	100	100	100	100	100	100	100	100
Hybrid CNN-LSTM [52]	97.14	97.6 [†]	97.59 [†]	97.43 [†]	99.99	100	99.99	99.99	100	100	100	100

[†] Although the authors explicitly reported the micro-average metrics, we include the weighted averages for consistency with the rest

B. RQ1: Validation Test

We evaluate the real-world feasibility of the FPA attack by conducting a testbed experiment in a controlled laboratory environment. Since industrial IoT networks are tightly regulated in nature, the following setup is designed to closely simulate practical scenarios.

Experimental Setup. Our experiment consists of two types of devices: a compromised MQTT client and an MQTT server. Since in this attack, it is assumed that an IIoT device is already affected, we choose a machine equipped with Ubuntu

24.04 (kernel version 6.11.0-26-generic) as the client, which is capable of crafting MQTT control packets. Regarding the MQTT server, a machine running Windows 11, version 24H2 (OS Build 26100.4349) is used. For both the client and the server, the *Eclipse Mosquitto* MQTT implementation is used separately. Following the proposed attack strategies, the client designs MQTT control packets and sends them to the installed Mosquitto server. To replicate an industrial IoT network environment, an access control list (ACL) is configured on the server side. Specifically, the access control policy topic `readwrite Building/Floor/+` is defined to grant the client permission to publish and subscribe to any topics that match this *single-level* topic pattern. To verify the correctness of the access control rule, we tested by sending PUBLISH packets with topics that violate the defined policy, and confirmed that the server correctly rejected these packets.

Attack Procedure. At the beginning of the attack, a TCP connection is automatically established by triggering the `socket.connect()` function call, and a carefully designed MQTT CONNECT packet is sent from the victim client. To prepare FPA packets in the proposed way, the `socket` networking library in Python (v3.12.3) is utilized for low-level TCP socket communication. It should be noted that all interactions with the MQTT server are performed on port 1883, which is the default port for MQTT over TCP without encryption. Notably, encrypted communication (i.e., port 8883) is *not* considered, as it alters the packet structure and conflicts with the features used to train the ML-NIDSs. To prevent unexpected connection drops, the Keep Alive interval is set to zero seconds, forcing the server to keep the connection alive for an unlimited time. After that, the crafted PUBLISH packets are continuously sent to the server. To make variations in the packets, the QoS bits and variable header contents are changed accordingly. Moreover, topic names and payload are generated in a systematic way described in § IV-C. Importantly, acceptance of these packets is verified by the PUBACK packets acknowledged by the server in response of PUBLISH with QoS=1. Additionally, the network log is also monitored from the server side. In total, we collect 167,121 network packets, including 83016 MQTT PUBLISH packets. During data collection, `Tcpdump` is used to capture traffic, and irrelevant packets are filtered out by applying `tcp port 1883`. The entire process takes 11 hours 29 minutes on a machine with an Intel Core i9-14900K CPU, 32 GB RAM, and 2.75 TB SSD. Finally, the captured network traffic is converted to `csv` format by extracting 61 features from the `pcap` file. Importantly, the extracted features and their data types are kept identical to those in the selected IIoT dataset, *Edge-IIoTset* [15] so that they can be tested with the ML-NIDSs without any compatibility issues.

C. RQ2: Effectiveness and Impact Analysis

We examine the effect of FPA by testing the ML-NIDSs with crafted packets generated in the previous section. First, the attack's effectiveness is measured using three metrics:

attack success rate (ASR), confidence score, and entropy. Next, its operational impact on the Security Operations Center is assessed by measuring the average waiting time.

Effectiveness Analysis: *Attack success rate* is the ratio of misclassified samples to the total number of attack samples. Let a preprocessed network traffic sample, \mathbf{x} , be fed into a neural network, which produces \mathbf{z} as the output of final-layer activation functions. This output is then passed through the softmax function to compute predictions for K classes as: $\hat{\mathbf{y}} = \sigma(\mathbf{z}) \in [0, 1]^K$. By definition, *confidence score* is the maximum class probability obtained from the softmax output, that is, $\max_i \sigma(\mathbf{z})_i$, where the i denotes the i^{th} class [53], [54]. In addition, we define *entropy* as the well-known Shannon entropy of the softmax distribution, $H(\sigma(\mathbf{z})) = -\sum_{i=1}^K \sigma(\mathbf{z})_i \log \sigma(\mathbf{z})_i$, which is used to measure the uncertainty of the predicted class probabilities. The higher the entropy, the more uncertain the prediction is. In this work, an ML-NIDS is reported as highly confident if its confidence score is greater than 0.9. Moreover, uncertainty is considered low when the entropy is below 0.5, and high when it exceeds 1.5. Although there is no standard threshold for low and high, we set them empirically to facilitate an in-depth analysis. Last but not least, a detection system is referred to as *overconfident* when its confidence score is high and uncertainty is low.

Table V-C shows the stats of the selected ML-NIDSs under attack. For the first ML-NIDS, *DCNNBiLSTM* [49], the attack success rate is 80.19%, where all FPA packets are misclassified as Uploading attack. Among the misclassified samples, 95.24% are predicted with high confidence, and 96.8% exhibit low entropy, highlighting the overconfidence of the neural network in nearly all cases. The statistics of average and geometric mean also support this result. The second ML-NIDS incorrectly classifies every FPA packet, however, into four different attack classes: Uploading, Password, Vulnerability_scanner, and XSS attack. Within the traffic mislabeled as Password, the model is overconfident in 11.79% instances; however, low entropy is observed in even more cases, signifying that the model is certain about its predictions despite showing less confidence. Among the packets misclassified as Vulnerability_scanner, in 4.7% cases, the model is overconfident. Interestingly, high-certainty predictions are found to be twice as common as high-confidence ones. For the remaining samples of this group, both the arithmetic and geometric means of the confidence and entropy are also moderate. Notably, the only FPA packet, incorrectly predicted as Uploading attack, is misclassified with poor confidence and high uncertainty. Although 2716 samples are incorrectly classified as XSS attacks, the model lacks confidence in these occurrences. Overall, this detection system is overconfident in 8.5% of cases during misclassifications. Turning to the next ML-NIDS, *SF-CNN-LSTM* [51], here the dominance of misclassifications towards the Uploading attack is also seen. Concerningly, the machine learning model is overconfident in 97.9% of situations. On average, the weighted means are 96%~97% and 0.04%~0.08% regarding confidence and entropy, respectively. A nearly identical pattern is observed in the last ML-NIDS, with slightly less (by 1%) confidence scores and more uncertainty than the previous one. However,

nearly all FPA attack packets are misclassified as Vulnerability_scanner attacks. Importantly, although this NIDS does not train on the MQTT-related features, the FPA attack still works due to the intra-packet dependencies, specifically, the reliance of the MQTT protocol on TCP.

TABLE II
EVALUATION OF ML-NIDS DURING FPA ATTACK. CONFIDENCE SCORE > 0.9 INDICATE HIGH CONFIDENCE; ENTROPY < 0.5 INDICATES LOW UNCERTAINTY, AND > 1.5 INDICATES HIGH UNCERTAINTY; OVERCONFIDENCE IS DEFINED AS CONFIDENCE SCORE > 0.9 WITH ENTROPY < 0.5

ML-NIDS	ASR (%) Misclassified as	# of Misclass.	Confidence		Entropy		# of High Conf.	# of Low/Hig. Entr.	# of Over Conf.
			μ	Geo. Conf.	μ	Geo. Entr.			
DCNN-BiLSTM [49]	80.19 Uploading	66570	0.979	0.977	0.077	0.031	63403	64436/0	63403
CNN-LSTM-GRU [50]	Uploading	1	0.237	0.237	1.673	1.673	0	0/1	0
	Password	45737	0.684	0.665	0.711	0.602	5391	86550/0	5391
	Vulnerability_scanner	34562	0.616	0.601	0.823	0.776	1626	3227/19	1626
	XSS	2716	0.518	0.509	1.010	0.983	0	0/141	0
		weighted μ		0.650	0.633	0.767	0.687		
SF-CNN-LSTM [51]	DDoS_HTTP	5762	0.767	0.746	0.544	0.453	2068	2577/0	2068
	Uploading	69920	0.994	0.993	0.021	0.003	68464	69374/0	68464
	XSS	7334	0.886	0.866	0.268	0.107	4984	5613/0	4984
			weighted μ		0.969	0.965	0.079	0.043	
Hybrid-CNN-LSTM [52]	DDoS_HTTP	6	0.694	0.668	0.728	0.672	0	2/0	0
	Password	140	0.897	0.878	0.327	0.010	90	96/0	90
	Uploading	329	0.680	0.670	0.783	0.770	0	0/1	0
	Vulnerability_scanner	82541	0.955	0.952	0.155	0.019	77538	78982/9	77538
		weighted μ		0.954	0.951	0.158	0.022		

Impact Analysis. To demonstrate the impact of FPA attacks in an industry-level Security Operations Center, we select the most relevant benchmark scenarios for MQTT use cases, *the enterprise set*. Specifically, *Fan-in connections* are employed, in which multiple publishers send MQTT PUBLISH messages to the server. According to the standards of popular platforms like Mosquitto and NanoMQ [55], 50K IIoT devices typically act as publishers, each sending one MQTT PUBLISH message per second. Considering the minimum false positive rates (80.12%) of the ML-NIDSs after launching FPA attack, we conduct a series of experiments with 1%, 5%, 10%, 15%, and 20% malicious devices, where the percentages of FPA alerts (fp) are 0.8012%, 4.006%, 8.012%, 12.018%, and 16.024%, respectively. However, before launching FPA, the false positive rate was 0%.

In this work, two sets of experiments are conducted using an M/D/c/FCFS queuing system, where attack alerts arrive in the service queue and a team of SOC analysts investigates them sequentially, each taking a deterministic amount of time [56], [57], [58]. The *budget* of the SOC team is defined as the maximum number of alerts the analysts can investigate per hour (a.k.a., service rate μ). *Alert arrival rate* is the total number of alerts arrived per hour, denoted as η . *Alert traffic intensity* is defined as the ratio of alert arrival rate and service rate, i.e., $\rho = \eta/\mu$. In both experiments, true positive alerts follow a Poisson distribution with an arrival rate of $\lambda = \eta * (1 - fp/100)$ and false positive alerts are evenly distributed in the system within time interval $[0, T]$, where T is the arrival time of the last true positive alert.

During the experiments, first, the arrival rate of the alerts is varied, keeping the budget fixed. Second, the budgets are varied, keeping the alert traffic intensity fixed. Regarding the first set of experiments, service time per alert is 30 sec, meaning that the team can investigate 120 alerts per hour, which is practical in real-world settings [57], [58]. However, the arrival rates of all alerts (η) are 115/hr, 116/hr, 117/hr, 118/hr, and 119/hr. Therefore, alert traffic intensity is $\rho < 1$,

representing a normal condition for the SOC. To observe the impact of false positive alerts, we measure *waiting time* of true positive alerts. Since true attack alerts arrive following a Poisson distribution and enter the queue server, each alert experiences a waiting time prior to investigation (which may sometimes be zero). Intuitively, the waiting time is expected to increase due to the injection of false positive alerts, since the time spent investigating these false alerts is entirely wasted, thereby delaying the servicing of genuine alerts. However, instead of reporting the waiting time for individual alerts, we present their cumulative waiting time. In addition, since the alerts follow specific distributions and may be subject to statistical bias, we run each experiment 10 times and report the average results. Moreover, we assess the impact over periods of one hour and one day. For the single-day test, the hourly arrival rate η and service rate μ are kept identical to maintain consistency.

As shown in Figures 5a and 5b, the presence of *intentional* FPA alerts increases the average waiting time of genuine alerts from 56.37 sec to 154.32 sec in one hour and from 9.49 hr to 11.41 hr in a single day, indicating that even attacking a small range of devices significantly degrades the performance of SOC team. The second set of experiments is conducted with different budgets, using service rates of 60, 80, 120, and 240 alerts/hr. The traffic intensity is maintained at a constant value of $\rho = 0.975$, observed to be suitable from previous experiments. According to Figures 5c and 5d, varying the budget does not notably change the impact of the proposed FPA attack, since the waiting time progressively increases as the number of false positive alerts grows.

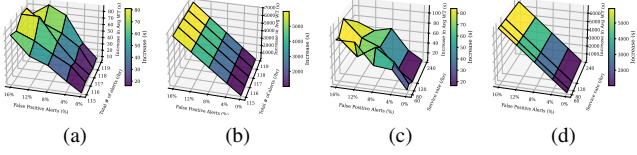


Fig. 5. (a)-(b) Fixed budget, varying alert traffic intensity: (a) 1 h, (b) 1 day; (c)-(d) Varying budget, fixed alert traffic intensity: (c) 1 h, (d) 1 day

Takeaway 1: All detection models have predominantly misclassified the crafted packets as the Uploading attack. In addition, half of them have been misled into considering these packets as Password, Vulnerability_scanner, XSS, and DDoS_HTTP attacks.

Takeaway 2: On a significant number of occasions, these systems demonstrate high confidence and low uncertainty during incorrect predictions. This is an alarming sign that the ML-NIDSs not only classify incorrectly but also are overconfident about the crafted FPA packets.

Takeaway 3: Experiments on a real-world enterprise set with different budgets and alert traffic intensities reveal that even a small number of false positive alerts (1% – 16%) substantially increase delays in investigating genuine alerts.

D. RQ3: Attack Analysis and XAI

In this section, we focus on analyzing FPA packets and investigating the reason for their misclassification, guided by three research questions. First, *how similar are the crafted FPA samples to the original MQTT samples?* By the term *similar*, we mean correlation similarity in a linear sense. Notably, the crafted packets are structurally similar, as the

FPA attack only affects the content of the packets, not their structure, and it is validated in § V-B. Second, *how far are the FPA samples from the original ones in the feature space?* Here, we consider both the crafted samples and their distribution. The final question is: *how does the deep learning model internally interpret high-dimensional network data, and which features most influence its predictions?* To address these questions, we adopt widely used statistical metrics and Explainable Artificial Intelligence (XAI) methods.

Similarity Analysis. Two popular correlation similarities – *Cosine similarity* and *Pearson product-moment correlation coefficient* (shortly, Pearson correlation, r) – are adopted to examine the similarity between FPA and unperturbed MQTT samples. *Cosine similarity* measures the angle between two vectors, indicating the directional alignment of these vectors. In contrast, the *Pearson correlation* is applied to assess the linear relationships between the vectors, where closer to 1 suggests a positive correlation, near 0 means little or no linear correlation, and close to -1 indicates a negative correlation. According to Table III, the cosine similarity and Pearson coefficient (r) between the original MQTT packets and the crafted FPA packets are 0.3987 and 0.3722, which highlights some sort of relatedness and a moderate level of similarity in the characteristic patterns. This result is intuitively correct, since the proposed FPA attack targets only a few specific fields of the network packet, rather than all. However, they are not closely aligned in direction. In contrast, considering the relationships with true attack classes, these measures are notably low, meaning that the feature vectors of the FPA samples have neither any linear relations nor any directional alignment with these attack samples.

TABLE III
SIMILARITY OF FPA SAMPLES WITH MQTT AND TRUE ATTACK

Metric	Class	Original MQTT	Uploading	Password	Vulnerability	XSS	DDoS HTTP
<i>Cosine similarity</i>		0.3987	0.054	0.0565	0.0714	0.0755	0.0821
<i>Pearson correlation</i>		0.3722	-0.0016	-0.0021	0.0112	0.0161	0.0247

Distance Analysis. Since similarity analysis did not yield any conclusive insights regarding the attack packets, we proceed with investigating the deviation and distributional difference between FPA and original packets. Specifically, three different distance metrics are employed: *Euclidean distance*, *Mahalanobis distance*, and *Kullback-Leibler (KL) divergence*. These distance metrics have been widely applied to vectors of any dimensionality or non-spatial data, especially in network traffic analysis, provided that the data are numerical [59], [60]. Whereas the *Euclidean* metric measures the distance between two vectors (e.g., the crafted and the original), *Mahalanobis* computes the distance of a vector (e.g., the crafted sample) from the center of a reference distribution (in this case, the distribution of original MQTT samples). Unlike Euclidean distance, which treats all features equally, Mahalanobis distance considers linear correlations among the features through a covariance matrix, and is considered to be more effective in various tasks [61], [62], [63].

Euclidean and Mahalanobis distance measures: While analyzing average Euclidean and Mahalanobis distances, the crafted packets are found to lie farther from the originals, around five times more than the true attack classes (see Figures 6a and 6b). In particular, the mean Euclidean and Mahalanobis distances for the FPA packets are 21.99 and 21992.11, respectively. On the other hand, the true attack classes are $3.93 \sim 4.253$ and $3909.11 \sim 4232.34$, far from the original MQTT samples. Importantly, the figures show that the individual FPA samples become closer to the true attack classes, indicating a possible reason for misclassification.

KL divergence analysis: After that, we extend our analysis by measuring the *KL divergence*, another well-known distance metric to quantify the distributional difference between the FPA and the original packets, and observe some sort of distance between these distributions in the feature space [64], [59]. First, we estimate their probability density functions (PDFs) using KDE (Kernel Density Estimation). Then, the KL divergence is computed. From Figure 6c, a noticeable discrepancy is observed in the distribution of the FPA data samples. In particular, the crafted FPA packets exhibit high divergence (0.6209) from the original ones, which implies a greater distributional shift. On the other hand, the true attack classes show low divergence (DDoS_HTTP: 0.0199, XSS: 0.0146, Vulnerability: 0.0145, Password: 0.0157, and Uploading: 0.0185), meaning that the distributions of the encoded true attack samples are likely to resemble the distribution of the original benign ones. It should be noted that this distributional similarity between the original benign and true attack is not unusual because the role of KL divergence is to measure the overall difference between probability distributions, not directly to separate different classes. However, advanced machine learning models, especially deep neural networks, can distinguish these true attacks, as they learn from complex and hierarchical representations of data.

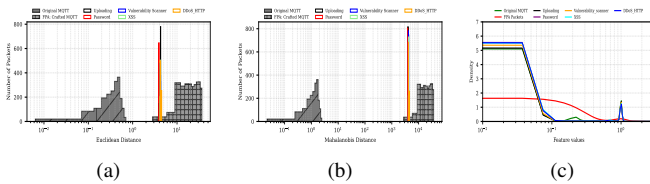


Fig. 6. Illustration of different distance measures, specifically (a) Euclidean distance, (b) Mahalanobis distance, and (c) KL divergence

Explainability Analysis. The *incomplete* findings of statistical analyses - particularly the unavailability of behavioral understanding for a specific model - motivate us to further analyze the explainability of ML-NIDSs. In particular, we leverage three fundamental principles for interpreting ML-based systems: *t-Distributed Stochastic Neighbor Embedding* (t-SNE), *Uniform Manifold Approximation and Projection* (UMAP), and *Shapley Additive exPlanations* (SHAP). The t-SNE is a dimensionality reduction technique, commonly used to visualize high-dimensional data in 2D or 3D space. The main purpose of adopting this technique is to capture the local structure of high-dimensional data [65]. Although UMAP is also used for dimensionality reduction, it can preserve

substantially more global structure than t-SNE [66]. However, these techniques can only illustrate how different data samples are close to each other and how different classes are distributed in feature space from the model's perspective, rather than providing any insight into which network features influence the predictions. To address this, we interpret the predictions of ML-NIDSs using a local explainability technique, SHAP, which quantifies the contribution of each feature to a particular prediction [67]. Depending on the importance of the features for the prediction, one SHAP value is assigned to each feature. A positive SHAP value (whether high or low) means the feature increases the model's prediction (i.e., a more important feature), a negative SHAP value decreases it, and a zero SHAP value indicates no contribution to the prediction.

t-SNE and UMAP analysis: To continue our investigation, we first select the best ML-NIDSs, *DCNNBiLSTM* [49], based on the lowest attack success rate (80.19%) and the highest performance. Next, we select a specific layer from the model, specifically *dense_2* layer, which is not close to the final prediction, but still provides a rich and meaningful representation of the data. The entire architecture of the model is provided in the Appendix (§F). From Figure 7a, we can observe a clear separation of classes, which indicates that the data samples belonging to the same class (with similar characteristics) are locally clustered together in the t-SNE space. However, this visualization does not provide concrete information about the possible cause of misclassification. Based on the efficacy observed from the previous statistical analyses, we generate two UMAP plots considering both Euclidean and Mahalanobis distances. The Euclidean UMAP shows significant overlaps of both the FPA and original MQTT clusters with the Uploading attack group (see Figure 7b). Although this result provides a better understanding of the internal representation of the data compared to t-SNE, the findings are not conclusive with respect to the misclassification. Interestingly, the UMAP, projected using the Mahalanobis distance metric, demonstrates that the FPA cluster partially overlaps with the Uploading attack group, whereas the original MQTT samples form a completely distinct cluster without any overlap (see Figure 7c).

SHAP analysis: Regarding the SHAP analysis, Figure 7d shows the SHAP beeswarm summary plot, representing the influence of the top ten features. Specifically, the figure reveals that the *mqtt.len* feature has the highest SHAP values, highlighting a significant role in increasing the predictions of *DCNNBiLSTM*. In addition, numerous red-colored points are observed for this feature, which signifies that the predictions are impacted by its high values. In other words, the (incorrect) predictions are affected by the packet padding strategy, hence, the FPA attack. A similar picture is seen for the *tcp.checksum*, which is also indirectly impacted by the proposed FPA attack, as described in § IV. However, the features with zero SHAP values do not contribute to the model predictions, for example, *tcp.len*, *mqtt.hdrflags*, *tcp.ack*, *tcp.ack_raw*, and *mqtt.topic-Temaprature_and_Humidity*. Other features, such as *tcp.seq* and *mqtt.topic_len* have a minimal impact on the predictions. Similar results, demonstrating the feature-level effects of the FPA attack, are observed while exploring the SHAP values for other ML-NIDSs (see Figure 10 in the Appendix).

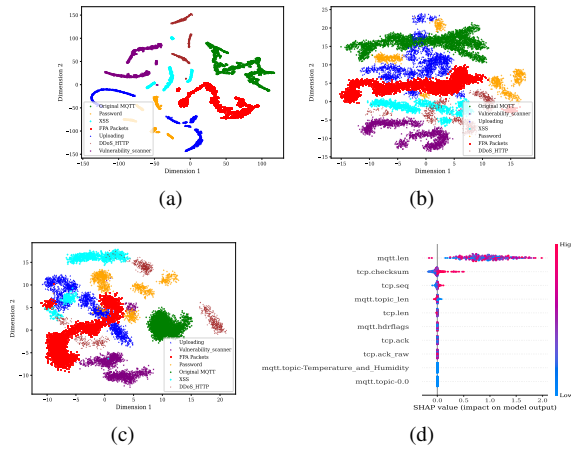


Fig. 7. First three Figures, (a) to (c), illustrate the machine learning model's internal representation of data using t-SNE and UMAP with (Euclidean and Mahalanobis) distance metrics. The last figure shows SHAP values of the top ten features influencing the misclassifications.

Takeaway 4: Analyses of the Mahalanobis distance and KL divergence provide strong evidence for a distributional shift in the FPA attack samples away from the original MQTT, importantly, closer to the true attack classes. This observation suggests that the FPA attack introduces exceptional but harmless patterns (i.e., *outliers*) in the network that match true attack samples in feature space to some extent.

Takeaway 5: From an ML explainability perspective, the adoption of the UMAP method using the Mahalanobis distance metric demonstrates a crucial overlap of the FPA cluster with the Uploading attack class in feature space, which indicates a potential misrepresentation of the FPA samples by the deep learning model.

Takeaway 6: The most influential features, identified through SHAP analysis, confirm that our FPA attack has effectively manipulated the model's behavior.

E. RQ4: Adversarial Training

In this research question, we explore the effectiveness of one of the most popular *adversarial training* techniques [19], [68], [6], [69], [70], [71] as a defense against FPA attack. More specifically, we aim to analyze whether the inclusion of adversarial samples enhances the robustness of the models. For this purpose, the *Edge-IoTset* dataset [15] is augmented with FPA attack packets.

Retraining and initial observation: Three different versions of each ML-NIDS are developed through adversarial retraining. Each version differs in the proportion of adversarial samples used during retraining. In particular, we take the ratio of crafted FPA samples and original MQTT samples as 5:100, 10:100, and 25:100, respectively. Following this, both the adversarial and original datasets are split into training-test sets with a standard ratio of 80:20, where the test portions from these datasets are defined as *robust test set* and *clean test set*, respectively. After adversarial training, we found that all versions can correctly classify FPA samples. However, some crucial deviations are observed in the clean test accuracy. Specifically, the precision, recall, and F1 scores of several classes fluctuate considerably. Since an in-depth analysis of *DCNNBiLSTM* [49] is conducted in the previous section, we continue exploring this system. However, the results of adversarial training for other NIDSs are provided in the

Appendix (Tables VII and VIII). It is worth mentioning that the fourth ML-NIDS, *Hybrid CNN-LSTM* [52], exhibits substantially degraded performance ($\sim 52.2\%$ accuracy) during adversarial training, even when 5% adversarial samples are used. A possible reason is the use of too limited a feature space, specifically only 18 features. Furthermore, we conduct an advanced test on these retrained ML-NIDSs, which can be found in the Appendix (see Table IX).

In-depth analysis: Table IV shows the clean test accuracies of all retrained versions of *DCNNBiLSTM*. Overall, the performance of adversarially trained models is slightly decreased in comparison to the original one. Among them, the second version has the smallest deviations for each metric across all classes (highlighted in the table). A closer examination of this model reveals that the precision of DDoS_TCP, Password, and Port_Scanning attacks is drastically decreased, specifically by 12%, 46%, and 99%, respectively. In addition, the per-class precision of Fingerprinting, Ransomware, Uploading, and XSS is also reduced. Considering the recall metric, a significant fall is identified in Port_Scanning ($\Delta = -51\%$) and SQL_injection ($\Delta = -73\%$) attack classes. The harmonic combination of these two metrics, the F1 score, is also notably dropped in eight classes, in total. However, for two classes: Fingerprinting and Ransomware attacks, the F1 score is improved by 8% and 1%, respectively. It should be noted that the severity of declination in the per-class performance is not reflected in overall statistics because of the class imbalance in the dataset, especially where the benign class dominates with consistently outstanding performance.

TABLE IV
CLEAN TEST ACCURACY OF THE RETRAINED *DCNNBiLSTM*

ID	Class	Before Adv. Training			After Adv. Training (# of adv. samples)			Support							
		prec.	rec.	F1	prec.	rec.	F1								
C0	Backdoor	95	98	97	95	98	97	97	4805						
C1	DDoS_HTTP	75	92	83	74	93	82	75	9709						
C2	DDoS_ICMP	100	100	100	99	100	100	100	13588						
C3	DDoS_TCP	83	100	91	71	100	83	71	100						
C4	DDoS_UDP	100	100	100	100	100	100	100	24314						
C5	Fingerprinting	73	48	58	61	62	61	67	171						
C6	MITM	100	100	100	100	100	99	100	72						
C7	Benign	100	100	100	100	100	100	100	272800						
C8	Password	90	14	24	43	84	57	44	987						
C9	Port_Scanning	99	51	68	0	0	0	0	3995						
C10	Ransomware	100	87	93	100	88	94	97	1938						
C11	SQL_injection	45	92	60	53	19	28	39	20165						
C12	Uploading	67	46	55	61	37	46	62	37						
C13	Vulnerability_scanner	95	85	90	94	84	89	84	10005						
C14	XSS	54	31	39	48	26	33	49	3013						
Weighted Avg. Delta		-	-	-	-2.586	-0.909	-1.176	-2.248	-0.739	-1.061	-2.668	-0.957	-1.129	381935	
Accuracy		0.95			0.94		0.94		0.94		0.94		0.94		381935

F. RQ5: Decision Boundary Analysis

Two important questions emerge from the results of adversarial training. First, *why does a small inclusion (even 5%) of adversarial examples during retraining make ML-NIDS fully robust to the FPA attack?* Second, *why does the performance for the true attack classes decrease significantly?* These two concerns lead to a deeper investigation, especially to analyze the change in the model's decision boundaries.

Decision boundaries on robust test set: To examine the decision boundaries learned by *DCNNBiLSTM*, we utilize a LogisticRegression model from the *scikit-learn* Python library and fit it to PCA-reduced data [72], [14]. The two side-by-side plots in Figure 8a show a shift in the boundaries after adversarial training, considering only the benign region and the Uploading (true) attack region, where the FPA packets were

misclassified before. Notably, the (red-colored) FPA samples lie deep into the true attack region, whereas the (green-colored) original MQTT samples are located near the boundary. This result may seem that the model is uncertain and lacks confidence about the class of the original samples, although they are correctly classified. However, we have found that the ML-NIDS shows 100% confidence and 0% entropy, signifying that it is overconfident about the original MQTT samples. Nevertheless, such closeness of original MQTT packets near the decision edge may be an important factor, implying why the FPA attack confuses ML-NIDSs. The right-hand plot in Figure 8a illustrates that after adversarial training, all data samples, including the FPA points, reside within their respective decision regions, which means that the neural network has learned a more stable decision boundary, especially for the benign class. To broaden our understanding, we plot a UMAP projection. As shown in Figure 8b, the FPA attack samples completely coincide with the original MQTT, indicating that the retrained model has effectively captured the underlying representation of the FPA data after adversarial training.

Decision boundaries on clean test set: Next, we explore how the model separates all classes (15) through its decision boundaries. Figures 8c and 8d show the corresponding visualizations before and after adversarial training, respectively. As illustrated in the figures, adversarial training has made

Password packets (8866) nearly accurately, but misclassifies SQL_injection as Password attack, in roughly 73% cases. The second noticeable point is that Figure 8d does not contain any decision region for the Port_Scanning attack (C9). The statistics in the confusion matrices also convey similar information, which indicates that the retrained model may not learn any meaningful patterns for this class. To further investigate the situation, we have closely inspected the dataset and found that four other classes - Fingerprinting, MITM, Ransomware, and XSS attacks - have fewer samples than the Port_Scanning class in both train and test sets, which signifies that *data imbalance* may not be the cause of such unexpected behavior. It should be noted that all of the Port_Scanning attack samples (3990) are misclassified as DDoS_TCP attack, although around 50% of these misclassifications also occurred before adversarial training. Another important observation is that the retrained model seems to learn more stable decision regions for some classes, especially Fingerprinting, MITM, and XSS, since these regions appear in the plot that was previously missing. However, some small discrepancies (1% ~ 8%) were found in their per-class precision, per-class recall, and per-class F1 score (see Table IV). Interestingly, adversarial training is often found to affect clean performance, and balancing this trade-off is a well-studied problem in the literature [73], [74].

Takeaway 7: Although retrained ML-NIDSs can correctly classify FPA samples, adversarial training brings several *negative side effects* to the models. Specifically, the underlying data appear to be badly misrepresented after retraining, leading to substantial performance degradations for a significant number of true attack classes.

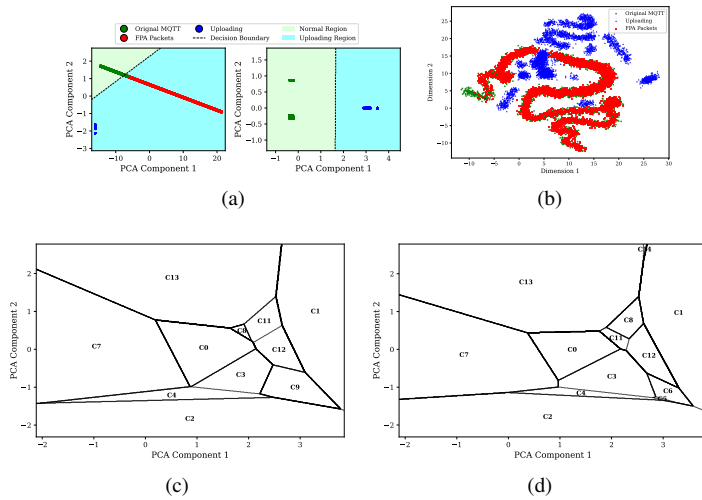


Fig. 8. Figure (a) shows the change in decision boundaries after retraining with highlighting the misclassified FPA samples (red-colored). The second figure provides an illustration of the model’s internal representation of data after retraining, where an overlap between the (previously) misclassified samples and the original MQTT samples is shown. Figures (c) and (d) exhibit a comparison of decision boundaries for all classes, before and after adversarial training.

some notable changes in the decision regions for several classes. First, the regions of the Password attack (C8) and the SQL_injection attack (C11) have been swapped and reshaped. To verify this, we compute the corresponding confusion matrices (see Figure 11). Before adversarial training, most of the Password attack samples (7761) are misclassified as SQL_injection, whereas the true SQL_injection attack is classified with minimal error. Interestingly, after adversarial training, the scenario is reversed. Now, the model can predict

VI. RELATED WORK

Adversarial Examples. In image classification tasks, it is well-established that small perturbations in input pixels can mislead neural networks to incorrectly label images, for example, an image of “Panda” is misclassified as “Gibbon”. These approaches often leverage linear perturbation [20], optimization-based methods [75], [76], [23], and GAN-based adversarial sample generation [77], [78]. Related to these, physical perturbations (e.g., overlaying and fabrication) in regulatory traffic signs can also cause misclassification; for instance, a “Stop” sign is incorrectly classified as a “Speed Limit” sign [79]. Note that these perturbation mechanisms are likely to violate constraints of the MQTT protocol when applied to IIoT networks. Another well-studied domain is malware detection, where executable binaries are obfuscated to bypass ML-based malware classifiers by adding API calls [80], [78], editing padding bytes [81], PE header bytes [82], or adding bogus code blocks [83], [84]. While these perturbation strategies are specific to binary rewriting, the perturbation proposed in this work is specified to MQTT protocol constraint violation-avoidance.

Evasion Attacks in NIDS. In the intrusion detection space, adversarial samples are generally attack traffic created or manipulated to bypass the detection model by being misclassified as *benign*. This is widely known as the *evasion attack*. Popular evasion strategies adopt GAN-based sample generation [1], [2], [3], gradient-based methods (Adaptive

JSMA [4], FGSM, BIM, PGD [5]), score-based methods (NES, OPT [6]), decision-based methods (Boundary attack, Pointwise attack, HopSkipJump attack [6]), and modification of raw network packets [7], [8], [9]. Unlike evasion attacks, in this work, we propose a counterintuitive FPR manipulation attack, where a *benign* network traffic is intentionally perturbed to be misclassified as an *attack*.

VII. CONCLUSION

This paper introduces a novel cyberattack in Industrial Internet of Things networks by systematically designing benign MQTT packets that can deceive machine learning-based network intrusion detection systems. The extensive evaluation demonstrates the effectiveness of the proposed attack. Further investigation reveals that popular defense approaches, particularly adversarial training, can mitigate the attack but give rise to some severe negative consequences.

REFERENCES

- [1] E. Alshahrani, D. Alghazzawi, R. Alotaibi, and O. Rabie, “Adversarial attacks against supervised machine learning based network intrusion detection systems,” *Plos one*, vol. 17, no. 10, p. e0275971, 2022.
- [2] W. Yao, H. Peng, Q. Li, and X. Shen, “Modeling realistic adversarial traffic against deep learning-based intrusion detection system in industrial IoT,” *IEEE Internet of Things Journal*, 2025.
- [3] Z. Lin, Y. Shi, and Z. Xue, “Idsgan: Generative adversarial networks for attack generation against intrusion detection,” in *Pacific-asia conference on knowledge discovery and data mining*. Springer, 2022, pp. 79–91.
- [4] R. Sheatsley, N. Papernot, M. J. Weisman, G. Verma, and P. McDaniel, “Adversarial examples for network intrusion detection systems,” *Journal of Computer Security*, vol. 30, no. 5, pp. 727–752, 2022.
- [5] O. Ibitoye, O. Shafiq, and A. Matrawy, “Analyzing adversarial attacks against deep learning for intrusion detection in IoT networks,” in *2019 IEEE global communications conference (GLOBECOM)*. IEEE, 2019, pp. 1–6.
- [6] C. Zhang, X. Costa-Perez, and P. Patras, “Adversarial attacks against deep learning-based network intrusion detection systems and defense mechanisms,” *IEEE/ACM Transactions on Networking*, vol. 30, no. 3, pp. 1294–1311, 2022.
- [7] Y. Sharon, D. Berend, Y. Liu, A. Shabtai, and Y. Elovici, “TANTRA: Timing-based adversarial network traffic reshaping attack,” *IEEE Transactions on Information Forensics and Security*, vol. 17, pp. 3225–3237, 2022.
- [8] M. J. Hashemi, G. Cusack, and E. Keller, “Towards evaluation of NIDSs in adversarial setting,” in *Proceedings of the 3rd ACM CoNEXT Workshop on Big DAta, Machine Learning and Artificial Intelligence for Data Communication Networks*, 2019, pp. 14–21.
- [9] H. Yan, X. Li, W. Zhang, R. Wang, H. Li, X. Zhao, F. Li, and X. Lin, “Automatic evasion of machine learning-based network intrusion detection systems,” *IEEE Transactions on Dependable and Secure Computing*, vol. 21, no. 1, pp. 153–167, 2023.
- [10] M. Roesch *et al.*, “Snort: Lightweight intrusion detection for networks.” in *Lisa*, vol. 99, no. 1, 1999, pp. 229–238.
- [11] V. Paxson, “Bro: a system for detecting network intruders in real-time,” *Computer networks*, vol. 31, no. 23-24, pp. 2435–2463, 1999.
- [12] M. Zolanvari, M. A. Teixeira, and R. Jain, “Effect of imbalanced datasets on security of industrial IoT using machine learning,” in *2018 IEEE international conference on intelligence and security informatics (ISI)*. IEEE, 2018, pp. 112–117.
- [13] M. S. Ahsan, S. Islam, and S. Shatabda, “A systematic review of metaheuristics-based and machine learning-driven intrusion detection systems in IoT,” *Swarm and Evolutionary Computation*, vol. 96, p. 101984, 2025.
- [14] K. He, D. D. Kim, and M. R. Asghar, “Adversarial machine learning for network intrusion detection systems: A comprehensive survey,” *IEEE Communications Surveys & Tutorials*, vol. 25, no. 1, pp. 538–566, 2023.
- [15] M. A. Ferrag, O. Friha, D. Hamouda, L. Maglaras, and H. Janicke, “Edge-IIoTset: A new comprehensive realistic cyber security dataset of IoT and IIoT applications for centralized and federated learning,” *IEEE Access*, vol. 10, pp. 40 281–40 306, 2022.
- [16] J. Ngawé, S. Sahoo, Y. Pequignot, F. Precioso, and C. Gagné, “Detecting brittle decisions for free: Leveraging margin consistency in deep robust classifiers,” *Advances in Neural Information Processing Systems*, vol. 37, pp. 23 301–23 324, 2024.
- [17] Y. Yang, R. Khanna, Y. Yu, A. Gholami, K. Keutzer, J. E. Gonzalez, K. Ramchandran, and M. W. Mahoney, “Boundary thickness and robustness in learning models,” *Advances in Neural Information Processing Systems*, vol. 33, pp. 6223–6234, 2020.
- [18] M. Khouri and D. Hadfield-Menell, “On the geometry of adversarial examples,” *arXiv preprint arXiv:1811.00525*, 2018.
- [19] Y. Xu, Y. Sun, M. Goldblum, T. Goldstein, and F. Huang, “Exploring and exploiting decision boundary dynamics for adversarial robustness,” *arXiv preprint arXiv:2302.03015*, 2023.
- [20] I. J. Goodfellow, J. Shlens, and C. Szegedy, “Explaining and harnessing adversarial examples,” *arXiv preprint arXiv:1412.6572*, 2014.
- [21] A. Madry, A. Makelov, L. Schmidt, D. Tsipras, and A. Vladu, “Towards deep learning models resistant to adversarial attacks,” *arXiv preprint arXiv:1706.06083*, 2017.
- [22] N. Papernot, P. McDaniel, S. Jha, M. Fredrikson, Z. B. Celik, and A. Swami, “The limitations of deep learning in adversarial settings,” in *2016 IEEE European symposium on security and privacy (EuroS&P)*. IEEE, 2016, pp. 372–387.
- [23] P.-Y. Chen, H. Zhang, Y. Sharma, J. Yi, and C.-J. Hsieh, “ZOO: Zeroth order optimization based black-box attacks to deep neural networks without training substitute models,” in *Proceedings of the 10th ACM workshop on artificial intelligence and security*, 2017, pp. 15–26.
- [24] W. Brendel, J. Rauber, and M. Bethge, “Decision-based adversarial attacks: Reliable attacks against black-box machine learning models,” *arXiv preprint arXiv:1712.04248*, 2017.
- [25] Z. Zhao, D. Dua, and S. Singh, “Generating natural adversarial examples,” *arXiv preprint arXiv:1710.11342*, 2017.
- [26] O. Standard, “MQTT version 3.1.1,” <http://docs.oasis-open.org/mqtt/mqtt/v3>, vol. 1, p. 29, 2014.
- [27] P. Colombo and E. Ferrari, “Access control enforcement within MQTT-based Internet of Things ecosystems,” in *Proceedings of the 23rd ACM on Symposium on Access Control Models and Technologies*, 2018, pp. 223–234.
- [28] HiveMQ Team, “Authorization – MQTT security fundamentals,” HiveMQ, 2024, [Online]. Available: <https://www.hivemq.com/blog/mqtt-security-fundamentals-authorization>.
- [29] Eclipse Mosquitto, “mosquitto.conf man page,” <https://mosquitto.org/man/mosquitto-conf-5.html>, [Online].
- [30] A. Hue, G. Sharma, and J.-M. Dricot, “Privacy-enhanced MQTT protocol for massive iot,” *Electronics*, vol. 11, no. 1, p. 70, 2021.
- [31] J. Nivethan and M. Papa, “On the use of open-source firewalls in IC/SCADA systems,” *Information Security Journal: A Global Perspective*, vol. 25, no. 1-3, pp. 83–93, 2016.
- [32] D. Scholz, D. Raumer, P. Emmerich, A. Kurtz, K. Lesiak, and G. Carle, “Performance implications of packet filtering with Linux eBPF,” in *2018 30th International Teletraffic Congress (ITC 30)*, vol. 1. IEEE, 2018, pp. 209–217.
- [33] O. N. Nyasore, P. Zavarsky, B. Swar, R. Naiyeju, and S. Dabra, “Deep packet inspection in industrial automation control system to mitigate attacks exploiting Modbus/TCP vulnerabilities,” in *2020 IEEE 6th Intl Conference on Big Data Security on Cloud (BigDataSecurity), IEEE Intl Conference on High Performance and Smart Computing,(HPSC) and IEEE Intl Conference on Intelligent Data and Security (IDS)*. IEEE, 2020, pp. 241–245.
- [34] R. T. El-Maghreby, N. M. Abd Elazim, and A. M. Bahaa-Eldin, “A survey on deep packet inspection,” in *2017 12th International Conference on Computer Engineering and Systems (ICCES)*. IEEE, 2017, pp. 188–197.
- [35] S. Lakshminarayana, A. Praseed, and P. S. Thilagam, “Securing the IoT application layer from an MQTT protocol perspective: Challenges and research prospects,” *IEEE Communications Surveys & Tutorials*, 2024.
- [36] G. Apruzzese, P. Laskov, E. Montes de Oca, W. Mallouli, L. Brdalo Rapa, A. V. Grammatopoulos, and F. Di Franco, “The role of machine learning in cybersecurity,” *Digital Threats: Research and Practice*, vol. 4, no. 1, pp. 1–38, 2023.
- [37] J. T. Hancock and T. M. Khoshgoftaar, “Survey on categorical data for neural networks,” *Journal of big data*, vol. 7, no. 1, p. 28, 2020.
- [38] H. Team, “MQTT Essentials: A Lightweight IoT Protocol,” HiveMQ, n.d., ch. 4, p. 15, [Online]. Available: <https://akhileshmoghe.github.io/assets/docs/iot/protocols/mqtt/hivemq-ebook-mqtt-essentials.pdf>.
- [39] S. Alcock and R. Nelson, “An analysis of TCP maximum segment sizes,” 2010.

[40] G. Huston, “TCP MSS values – what’s changed?” APNIC Blog, Jul 2019, [Online]. Available: <https://blog.apnic.net/2019/07/31/tcp-mss-values-whats-changed/>.

[41] J. Postel, “Transmission Control Protocol,” IETF, RFC 793, Sep. 1981, section 3.1. [Online]. Available: <https://www.rfc-editor.org/info/rfc793>

[42] A. L. Buczak and E. Guven, “A survey of data mining and machine learning methods for cyber security intrusion detection,” *IEEE Communications surveys & tutorials*, vol. 18, no. 2, pp. 1153–1176, 2015.

[43] M. Tavallaei, E. Bagheri, W. Lu, and A. A. Ghorbani, “A detailed analysis of the KDD CUP 99 data set,” in *2009 IEEE symposium on computational intelligence for security and defense applications*. IEEE, 2009, pp. 1–6.

[44] N. Moustafa and J. Slay, “UNSW-NB15: a comprehensive data set for network intrusion detection systems (UNSW-NB15 network data set),” in *2015 military communications and information systems conference (MilCIS)*. IEEE, 2015, pp. 1–6.

[45] N. Koroniotis, N. Moustafa, E. Sitnikova, and B. Turnbull, “Towards the development of realistic botnet dataset in the internet of things for network forensic analytics: Bot-IoT dataset,” *Future Generation Computer Systems*, vol. 100, pp. 779–796, 2019.

[46] I. Sharafaldin, A. H. Lashkari, A. A. Ghorbani *et al.*, “Toward generating a new intrusion detection dataset and intrusion traffic characterization,” *ICISSP*, vol. 1, pp. 108–116, 2018.

[47] N. Moustafa, “A new distributed architecture for evaluating AI-based security systems at the edge: Network TON_IoT datasets,” *Sustainable Cities and Society*, vol. 72, p. 102994, 2021.

[48] Y. Meidan, M. Bohadana, Y. Mathov, Y. Mirsky, A. Shabtai, D. Breitenbacher, and Y. Elovici, “N-BaIoT—network-based detection of IoT botnet attacks using deep autoencoders,” *IEEE Pervasive Computing*, vol. 17, no. 3, pp. 12–22, 2018.

[49] V. Hnamte and J. Hussain, “DCNNBiLSTM: An efficient hybrid deep learning-based intrusion detection system,” *Telematics and Informatics Reports*, vol. 10, p. 100053, 2023.

[50] D. Kilichev, D. Turimov, and W. Kim, “Next-generation intrusion detection for IoT EVCS: Integrating CNN, LSTM, and GRU models,” *Mathematics*, vol. 12, no. 4, p. 571, 2024.

[51] F. Imani, M. Kargar, A. Assadzadeh, and A. Bayani, “Integrating CNN-LSTM networks with statistical filtering techniques for intelligent IoT intrusion detection,” in *2024 8th International Conference on Smart Cities, Internet of Things and Applications (SCIoT)*. IEEE, 2024, pp. 189–195.

[52] E. M. de Elias, V. S. Carriel, G. W. De Oliveira, A. L. Dos Santos, M. Nogueira, R. H. Junior, and D. M. Batista, “A hybrid CNN-LSTM model for IIoT edge privacy-aware intrusion detection,” in *2022 IEEE Latin-American Conference on Communications (LATINCOM)*. IEEE, 2022, pp. 1–6.

[53] D. Hendrycks and K. Gimpel, “A baseline for detecting misclassified and out-of-distribution examples in neural networks,” *arXiv preprint arXiv:1610.02136*, 2016.

[54] T. Pearce, A. Brintrup, and J. Zhu, “Understanding softmax confidence and uncertainty,” 2021.

[55] May Jin, “Open MQTT Benchmarking Comparison: Mosquitto vs NanoMQ,” <https://www.emqx.com/en/blog/open-mqtt-benchmarking-comparison-mosquitto-vs-nanomq>, [Online].

[56] A. Shah, R. Ganesan, S. Jajodia, and H. Cam, “Understanding tradeoffs between throughput, quality, and cost of alert analysis in a csoc,” *IEEE Transactions on Information Forensics and Security*, vol. 14, no. 5, pp. 1155–1170, 2018.

[57] —, “A methodology to measure and monitor level of operational effectiveness of a csoc,” *International Journal of Information Security*, vol. 17, no. 2, pp. 121–134, 2018.

[58] L. Yang, Z. Chen, C. Wang, Z. Zhang, S. Booma, P. Cao, C. Adam, A. Withers, Z. Kalbarczyk, R. K. Iyer *et al.*, “True attacks, attack attempts, or benign triggers? an empirical measurement of network alerts in a security operations center,” in *33rd USENIX Security Symposium (USENIX Security 24)*, 2024, pp. 1525–1542.

[59] D. J. Weller-Fahy, B. J. Borghetti, and A. A. Sodemann, “A survey of distance and similarity measures used within network intrusion anomaly detection,” *IEEE Communications Surveys & Tutorials*, vol. 17, no. 1, pp. 70–91, 2014.

[60] D. H. Hoang and H. D. Nguyen, “A PCA-based method for IoT network traffic anomaly detection,” in *2018 20th International conference on advanced communication technology (ICACT)*. IEEE, 2018, pp. 381–386.

[61] G. J. McLachlan, “Mahalanobis distance,” *Resonance*, vol. 4, no. 6, pp. 20–26, 1999.

[62] K. Lee, K. Lee, H. Lee, and J. Shin, “A simple unified framework for detecting out-of-distribution samples and adversarial attacks,” *Advances in neural information processing systems*, vol. 31, 2018.

[63] S. Xiang, F. Nie, and C. Zhang, “Learning a mahalanobis distance metric for data clustering and classification,” *Pattern recognition*, vol. 41, no. 12, pp. 3600–3612, 2008.

[64] I. Goodfellow, Y. Bengio, and A. Courville, *Deep Learning*. MIT Press, 2016, pp. 71–77. [Online]. Available: <http://www.deeplearningbook.org>.

[65] L. v. d. Maaten and G. Hinton, “Visualizing data using t-SNE,” *Journal of machine learning research*, vol. 9, no. Nov, pp. 2579–2605, 2008.

[66] L. McInnes, J. Healy, and J. Melville, “UMAP: Uniform manifold approximation and projection for dimension reduction,” *arXiv preprint arXiv:1802.03426*, 2018.

[67] S. M. Lundberg and S.-I. Lee, “A unified approach to interpreting model predictions,” *Advances in neural information processing systems*, vol. 30, 2017.

[68] M. Pawlicki, M. Choraś, and R. Kozik, “Defending network intrusion detection systems against adversarial evasion attacks,” *Future Generation Computer Systems*, vol. 110, pp. 148–154, 2020.

[69] M. Usama, M. Asim, S. Latif, J. Qadir *et al.*, “Generative adversarial networks for launching and thwarting adversarial attacks on network intrusion detection systems,” in *2019 15th international wireless communications & mobile computing conference (IWCMC)*. IEEE, 2019, pp. 78–83.

[70] A. Shafahi, M. Najibi, M. A. Ghiasi, Z. Xu, J. Dickerson, C. Studer, L. S. Davis, G. Taylor, and T. Goldstein, “Adversarial training for free!” *Advances in neural information processing systems*, vol. 32, 2019.

[71] E. Wong, L. Rice, and J. Z. Kolter, “Fast is better than free: Revisiting adversarial training,” *arXiv preprint arXiv:2001.03994*, 2020.

[72] I. T. Jolliffe and J. Cadima, “Principal component analysis: a review and recent developments,” *Philosophical transactions of the royal society A: Mathematical, Physical and Engineering Sciences*, vol. 374, no. 2065, p. 20150202, 2016.

[73] D. Tsipras, S. Santurkar, L. Engstrom, A. Turner, and A. Madry, “Robustness may be at odds with accuracy,” *arXiv preprint arXiv:1805.12152*, 2018.

[74] T. Bai, J. Luo, J. Zhao, B. Wen, and Q. Wang, “Recent advances in adversarial training for adversarial robustness,” *arXiv preprint arXiv:2102.01356*, 2021.

[75] Y. Liu, X. Chen, C. Liu, and D. Song, “Delving into transferable adversarial examples and black-box attacks,” *arXiv preprint arXiv:1611.02770*, 2016.

[76] N. Carlini and D. Wagner, “Towards evaluating the robustness of neural networks,” in *2017 ieee symposium on security and privacy (sp)*. Ieee, 2017, pp. 39–57.

[77] C. Xiao, B. Li, J.-Y. Zhu, W. He, M. Liu, and D. Song, “Generating adversarial examples with adversarial networks,” *arXiv preprint arXiv:1801.02610*, 2018.

[78] W. Hu and Y. Tan, “Generating adversarial malware examples for black-box attacks based on GAN,” in *International Conference on Data Mining and Big Data*. Springer, 2022, pp. 409–423.

[79] I. Evtimov, K. Eykholt, E. Fernandes, T. Kohno, B. Li, A. Prakash, A. Rahmati, and D. Song, “Robust physical-world attacks on machine learning models,” *arXiv preprint arXiv:1707.08945*, vol. 2, no. 3, p. 4, 2017.

[80] I. Rosenberg, A. Shabtai, L. Rokach, and Y. Elovici, “Generic black-box end-to-end attack against state of the art API call based malware classifiers,” in *International Symposium on Research in Attacks, Intrusions, and Defenses*. Springer, 2018, pp. 490–510.

[81] B. Kolosnjaji, A. Demontis, B. Biggio, D. Maiorca, G. Giacinto, C. Eckert, and F. Roli, “Adversarial malware binaries: Evading deep learning for malware detection in executables,” in *2018 26th European signal processing conference (EUSIPCO)*. IEEE, 2018, pp. 533–537.

[82] L. Demetrio, B. Biggio, G. Lagorio, F. Roli, and A. Armando, “Explaining vulnerabilities of deep learning to adversarial malware binaries,” *arXiv preprint arXiv:1901.03583*, 2019.

[83] F. Pierazzi, F. Pendlebury, J. Cortellazzi, and L. Cavallaro, “Intriguing properties of adversarial ML attacks in the problem space,” in *2020 IEEE symposium on security and privacy (SP)*. IEEE, 2020, pp. 1332–1349.

[84] L. Zhang, P. Liu, Y.-H. Choi, and P. Chen, “Semantics-preserving reinforcement learning attack against graph neural networks for malware detection,” *IEEE Transactions on Dependable and Secure Computing*, vol. 20, no. 2, pp. 1390–1402, 2022.

[85] J. Kinyua and L. Awuah, “AI/ML in security orchestration, automation and response: Future research directions.” *Intelligent Automation & Soft Computing*, vol. 28, no. 2, 2021.

[86] C. Islam, M. A. Babar, and S. Nepal, "A multi-vocal review of security orchestration," *ACM Computing Surveys (CSUR)*, vol. 52, no. 2, pp. 1–45, 2019.

[87] E. Jackson and R. Agrawal, "Performance evaluation of different feature encoding schemes on cybersecurity logs," in *2019 SoutheastCon*, 2019, pp. 1–9.

[88] F. Tramèr, F. Zhang, A. Juels, M. K. Reiter, and T. Ristenpart, "Stealing machine learning models via prediction {APIs}, " in *25th USENIX security symposium (USENIX Security 16)*, 2016, pp. 601–618.

APPENDIX

A. Example Usage of Wildcards in ACL

In the single-level wildcard, denoted by `+`, exactly one level in the topic is matched. For example, an Access Control List (ACL) rule `"factory/+humidity"` matches topics like `factory/line1/humidity` and `factory/line2/humidity`, but not `factory/line1/sectionA/humidity`, `factory/line1/humidity/sectionB`, or `factory/humidity`. On the other hand, the multi-level wildcard (`#`) matches any number of levels, including the parent (root) and any number of child (subordinate) levels. For instance, the rule `"factory/#"` matches `factory/line1`, `factory/line1/humidity`, `factory/line2/sectionB/temperature`, and any other topic that starts with `factory/` and `factory` itself.

B. Workflow of SOC During FPA

To understand the severity of the FPA attack and its effects on an ML-NIDS placed in a Security Operations Center (SOC), it is necessary to describe the workflow in the SOC. When our legitimately designed *benign* MQTT PUBLISH packet traverses the IIoT network, the machine learning-based NIDS captures it and incorrectly classifies it as *attack* after appropriate preprocessing. Then, the SIEM (Security Information and Events Management) system generates an attack alert based on the security event triggered by the intrusion detection system. Subsequently, the SOAR (Security Orchestration, Automation, and Response) system retrieves the alert and sends notifications to the SOC analytic team with prediction results and other system reports [85], [86]. After conducting a manual investigation, security analysts determine that the alert is a *false positive*. In practice, the industry has widely integrated such ML-NIDSs with SOAR solutions in their security operations center. FireEye, IBM Resilient, Splunk, Siemplify, and Rapid7 are among the most prominent platforms. Figure 9 illustrates the events of the security operations center during a FPR manipulation attack.

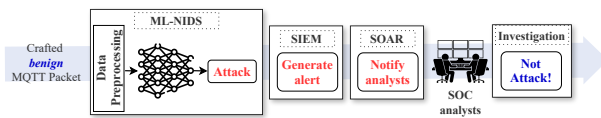


Fig. 9. Events of the SOC during FPR manipulation attack

C. A Conceptual Explanation of Possible Impact of the Proposed Topic Generation

Let's see an example of the most popular and efficient one-hot encoding technique [87], [88]. Say, the training dataset consists of m features as follows: $\langle F_1, F_2, \dots, TOPIC, \dots, F_m \rangle$

and the feature $TOPIC$ has three categorical values: $\{x, y, z\}$. Now, after one-hot encoding, the feature space becomes: $\langle F_1, F_2, \dots, topic_x, topic_y, topic_z, \dots, F_m \rangle$, where each new (binary) feature indicates the presence (1) or absence (0) of a specific category in the original $TOPIC$ feature. Assume that for three MQTT packets (data samples), the existing encoded patterns are: $[f_1, f_2, \dots, 1, 0, 0, \dots, f_m]$, $[f_1, f_2, \dots, 0, 1, 0, \dots, f_m]$, and $[f_1, f_2, \dots, 0, 0, 1, \dots, f_m]$. Using our padding strategy, the categorical values in the crafted samples will be: $\{x, x, x, \dots, x, \dots, y, y, y, \dots, z, z, z, \dots, z, z, z\}$, where `' '` denotes a whitespace. After encoding, the feature space is extended and possible sequences can be like: $[f_1, f_2, \dots, 0, 1, 0, 0, 0, 0, 0, 0, 0, 0, 0, 0, 0, 0, 0, \dots, f_m]$, $[f_1, f_2, \dots, 0, 0, 0, 0, 0, 0, 0, 1, 0, 0, 0, 0, 0, 0, 0, \dots, f_m]$, and $[f_1, f_2, \dots, 0, 0, 0, 0, 0, 0, 0, 0, 0, 0, 0, 1, 0, 0, \dots, f_m]$. Clearly, such padding distorts the feature patterns, even if the new features are dropped after preprocessing, and the impact can be more severe if the feature ($TOPIC$) is particularly influential in the dataset.

D. Features in the IIoT Dataset

Table V outlines 61 features (except label) extracted in the Edge-IIoTset [15] dataset.

TABLE V
PROTOCOL FEATURES WITH ASSIGNED FEATURE IDs

Protocol	Features (ID)
Frame	frame.time (F1)
IP	ip.src_host (F2), ip.dst_host (F3)
ARP	arp.dstproto_ip4 (F4), arp.opcode (F5), arp.hw.size (F6), arp.srcproto_ip4 (F7)
ICMP	icmp.checksum (F8), icmp.seq_le (F9), icmp.transmit_timestamp (F10), icmp.unused (F11)
HTTP	http_file_data (F12), http.content_length (F13), http.request.uri.query (F14), http.request.method (F15), http.referrer (F16), http.request.full_uri (F17), http.request.version (F18), http.response (F19), http.tls_port (F20)
TCP	tcp.ack (F21), tcp.ack_raw (F22), tcp.checksum (F23), tcp.connection.fin (F24), tcp.connection.rst (F25), tcp.connection.syn (F26), tcp.connection.synack (F27), tcp.dsport (F28), tcp.flags (F29), tcp.flags.ack (F30), tcp.len (F31), tcp.options (F32), tcp.payload (F33), tcp.seq (F34), tcp.sport (F35)
UDP	udp.port (F36), udp.stream (F37), udp.time_delta (F38), dns.qry.name (F39), dns.qry.name.len (F40)
DNS	dns.qry.qn (F41), dns.qry.type (F42), dns.retransmission (F43), dns.retransmit_request (F44), dns.retransmit_request_in (F45)
MQTT	mqtt.conack.flags (F46), mqtt.conflag.cleansess (F47), mqtt.conflags (F48), mqtt.hdrflags (F49), mqtt.len (F50), mqtt.msg_decoded_as (F51), mqtt.msg (F52), mqtt.msghype (F53), mqtt.proto_len (F54), mqtt.proto_name (F55), mqtt.topic (F56), mqtt.topic_len (F57), mqtt.ver (F58)
Modbus/TCP	mbtcp.len (F59), mbtcp.trans_id (F60), mbtcp.uni_id (F61)
Label	Attack_label (F62), Attack_type (F63)

E. The List of Features Used by the Selected ML-NIDSs

Table VI shows the total number of features and the list of TCP-MQTT feature IDs used by ML-NIDSs.

TABLE VI
ML-NIDSs AND THEIR USED FEATURE IDs [HIGHLIGHTED ONES ARE AFFECTED BY FPR MANIPULATION ATTACK]

ML-NIDS	Total # of Feat. used	TCP Features (IDs)	MQTT Features (IDs)
DCNNBILSTM [49]	46	F21, F22, F23, F24, F25, F46, F47, F48, F49, F50, F26, F27, F29, F30, F31 , F51, F53, F54, F55, F56 , F34	F57, F58
CNN-LSTM-GRU [50]	49	F21, F22, F23, F24, F25, F46, F47, F48, F49 , F50 , F26, F27, F28, F29, F30, F31 , F51, F53, F54, F55, F56 , F34	F57, F58
SF-CNN-LSTM [51]	46	21, F22, F23, F24, F25, F46, F47, F48, F49 , F50 , F26, F27, F29, F30, F31 , F51, F53, F54, F55, F56 , F34	F57, F58
Hybrid CNN-LSTM [52]	18	F21, F22, F23, F24, F25, F46, F47, F48, F49 , F50 , F26, F27, F29, F30, F31 , F54	-
			F57, F58, F34

F. Architecture of DCNNBiLSTM with Learned Parameters

The architecture of the best ML-NIDS, *DCNNBiLSTM* [49] is as follows: *conv1d* (*None*, 92, 96) \rightarrow *batch_normalization* (*None*, 92, 96) \rightarrow *bidirectional* (*None*, 192) \rightarrow *reshape* (*None*, 192, 1) \rightarrow *batch_normalization_1* (*None*, 192, 1) \rightarrow *bidirectional_1* (*None*, 256) \rightarrow *dense* (*None*, 64) \rightarrow *dropout* (*None*, 64) \rightarrow *dense_1* (*None*, 32) \rightarrow *dropout_1* (*None*, 32) \rightarrow *dense_2* (*None*, 16) \rightarrow *dropout_2* (*None*, 16) \rightarrow *dense_3* (*None*, 15) \rightarrow *activation* (*None*, 15). Specifically, the model combines one 1D convolution layer and two bidirectional LSTM layers, including other associates such as dense, Z-score normalization, dropout, and ReLu activations. In total, 308241 parameters are learned during training, whereas 194 are non-trainable and remain fixed.

G. SHAP Analysis of other ML-NIDSs under FPA

The plots in Figures 10 illustrate the top ten features influencing the incorrect predictions of ML-NIDSs: *CNN-LSTM-GRU* [50], *SF-CNN-LSTM* [51], and *Hybrid CNN-LSTM* [52], during FPA. Among these features, *mqtt.len*, *tcp.len*, *mqtt.topic_len*, and *tcp.checksum* are dominant, indicating the impact of FPA in deceiving machine learning models.

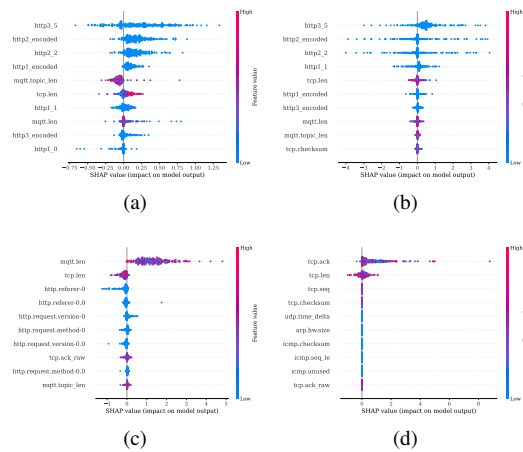


Fig. 10. SHAP beeswarm summary plots of other machine learning-based ML-NIDSs. Figures 10a and 10b represent the features that impact the second ML-NIDS to misclassify the FPA samples as Password and Vulnerability_scanner attacks. Subsequently, Figure 10c highlights the features influencing the third system to predict incorrectly as the Uploading class, whereas Figure 10d illustrates the SHAP values contributing to misclassification as the Vulnerability_scanner class by the fourth model.

H. Clean Test Accuracies of other ML-NIDSs

The per-class metrics for *CNN-LSTM-GRU* and *SF-CNN-LSTM* are reported in Tables VII and VIII. For *CNN-LSTM-GRU*, the overall performance is increased after adversarial training, whereas for *SF-CNN-LSTM* it is decreased. However, it should be noted that the changes in per-class statistics are not as visible due to the dominance of the benign class.

TABLE VII
CLEAN TEST ACCURACY OF *CNN-LSTM-GRU* [50]

ID	Class	Before Adv. Training			After Adv. Training (# of adv. samples)			25:100 (20754)			Support
		prec.	rec.	F1	prec.	rec.	F1	prec.	rec.	F1	
C0	Backdoor	95	95	95	97 \dagger	96 \dagger	96 \dagger	97	97	97	4805
C1	DDoS_HTTP	94	90	92	93 \dagger	91 \dagger	92	98	94	94	9709
C2	DDoS_ICMP	99	100	99	99	100	100	99	100	100	13588
C3	DDoS_TCP	97	93	95	97	94 \dagger	95	97	93	95	10012
C4	DDoS_UDP	100	100	100	100	100	100	100	100	100	24313
C5	Fingerprinting	100	26	41	95 \dagger	25 \dagger	39 \dagger	100	21	35	171
C6	MITM	100	100	100	100	100	100	100	100	100	72
C7	Benign	100	100	100	100	100	100	100	100	100	279925
C8	Password	55	80	65	54 \dagger	80	65	57	73	64	92
C9	Port_Scanning	85	100	92	86 \dagger	99 \dagger	92	85	100	92	3995
C10	Ransomware	97	83	89	99 \dagger	86 \dagger	92 \dagger	100	88	93	100
C11	SQL_injection	31	48	68	79 \dagger	58	67	71	66	68	1938
C12	Uploading	99	67	77	91 \dagger	67	77	92	66	77	1005
C13	Vulnerability_scanner	86	97	92	99 \dagger	92 \dagger	96 \dagger	99	92	96	95
C14	XSS	72	52	60	65 \dagger	82 \dagger	73 \dagger	66	66	66	3014
Weighted Average Delta		-	-	-	0.2389	0.1788	0.2038	0.0058	0.1374	0.1407	0.5895
Accuracy		-	-	-	0.97	0.97	0.97	0.97	0.97	0.97	389090

TABLE VIII
CLEAN TEST ACCURACY OF *SF-CNN-LSTM* [51]

ID	Class	Before Adv. Training			After Adv. Training (# of adv. samples)			25:100 (20754)			Support
		prec.	rec.	F1	prec.	rec.	F1	prec.	rec.	F1	
C0	Backdoor	95	97	96	95	98	97	96 \dagger	98	97	4805
C1	DDoS_HTTP	75	93	83	75	91	82	75	93	83	9709
C2	DDoS_ICMP	100	100	100	100	100	100	100	100	100	13588
C3	DDoS_TCP	82	100	90	71	100	83	71 \dagger	100	83 \dagger	100
C4	DDoS_UDP	100	100	100	100	100	100	100	100	100	24312
C5	Fingerprinting	87	63	73	76	41	53	65 \dagger	36 \dagger	47 \dagger	70
C6	MITM	100	93	96	100	100	100	100 \dagger	100	100	100
C7	Benign	100	100	100	100	100	100	100	100	100	100
C8	Password	92	48	27	44	88	59	44 \dagger	89 \dagger	59 \dagger	45
C9	Port_Scanning	100	48	65	60	0	0	0	0	0	3995
C10	Ransomware	97	86	91	99	88	93	99 \dagger	88 \dagger	94 \dagger	100
C11	SQL_injection	45	91	60	61	20	30	63 \dagger	19 \dagger	29 \dagger	46
C12	Uploading	67	48	56	60	34	44	60 \dagger	35 \dagger	44 \dagger	44
C13	Vulnerability_scanner	94	85	89	94	85	89	84 \dagger	89	94	85
C14	XSS	51	28	36	46	30	36	49 \dagger	25 \dagger	33 \dagger	27
Weighted Avg. Delta		-	-	-	-2.333	-0.088	-1.067	-2.248	-0.798	-1.09	-0.0811
Accuracy		-	-	-	0.95	0.94	0.94	0.94	0.94	0.94	381935

I. Advanced Robustness Test

To check whether adversarially trained models can handle MQTT packets with unseen topics, we randomly generated topics while crafting the FPA packets, keeping other parts consistent with the procedure described in § IV. In particular, first, a set of topic names is extracted from the publicly available IIoT datasets. Then, a tokenization approach is devised, where each retrieved topic is split by slash (/), underscore (), and whitespace. For example, after tokenization, the topic *Soil_Sensor* is broken down into *(Soil)*, and *(Sensor)* tokens. Next, a new topic is created by randomly selecting from the tokens. In this way, the new topics remain meaningful yet random. Regarding the MQTT server, we experimented with two popular public MQTT brokers from Mosquitto and HiveMQ. Their corresponding domains (and IPs during testing) are: “*test.mosquitto.org*” (5.196.78.28) and ‘*broker.hivemq.com*’ (3.126.159.86). However, for this experiment, the ACL rule is not considered. The test results in Table IX demonstrate that while the first and third ML-NIDSs - *DCNNBiLSTM* [49], *SF-CNN-LSTM* [51] - exhibit perfect accuracy, precision, recall, and F1 scores, the second one: *CNN-LSTM-GRU* [50] significantly underperforms.

TABLE IX
RESULTS OF ADVANCED ROBUSTNESS TEST

ML-NIDS	acc	prec	rec	F1
DCNNBiLSTM [49]	100	100	100	100
CNN-LSTM-GRU [50]	34.7	100	34.7	51.52
SF-CNN-LSTM [51]	100	100	100	100

J. Confusion Matrices of the ML-NIDSs

The confusion matrices in Figures (11)-(13) are presented side-by-side to compare classification performances before and

after adversarial training. The matrices related to the first ML-NIDS are already described in § V. Regarding the second one, *CNN-LSTM-GRU*, no notable changes are observed in the matrices. However, per-class performance of the retrained *SF-CNN-LSTM* is noticeably altered. First, the statistics of the Password attack (C8) and the SQL_injection (C11) are replaced. Second, all Port_Scanning samples are misclassified as DDoS_TCP. These two modified behaviors are also found in the case of the first ML-NIDS, *DCNNBiLSTM*. However, an extra crucial deviation is observed here, especially for the Uploading attack class (C12). Before adversarial training, half of its samples were misclassified as SQL_injection (C11), whereas, after retraining, more than 50% samples are misclassified as the Password attack (C8). It is worth mentioning that this model misclassified most of the FPA attacks as Uploading before retraining (see Table V-C). Another important point is that although adversarial training does not affect the per-class metrics of the second ML-NIDS, according to the results of the advanced test (Table IX), the system is not robust enough.

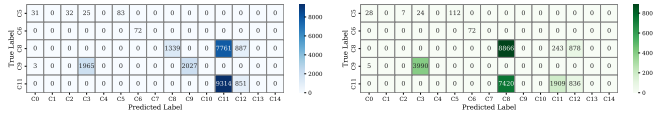


Fig. 11. Confusion matrices for *DCNNBiLSTM* before (left) and after (right) adversarial training. Since the corresponding decision boundaries are already analyzed in § V, only the classes with significant deviations are shown.

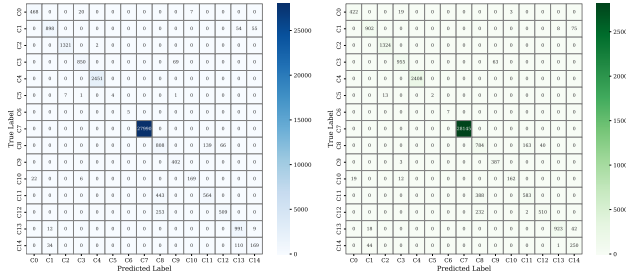


Fig. 12. Confusion matrices for *CNN-LSTM-GRU* before (left) and after (right) adversarial training

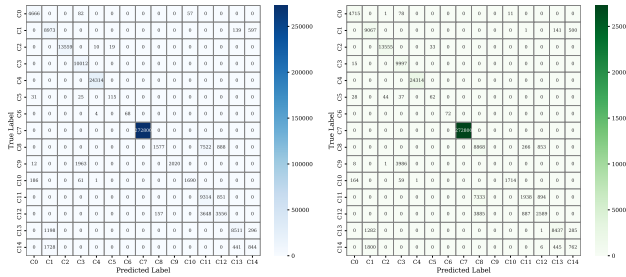


Fig. 13. Confusion matrices for *SF-CNN-LSTM* before (left) and after (right) adversarial training